Physics – Uspekhi **67** (2) 109 – 128 (2024) ©2024 Uspekhi Fizicheskikh Nauk, Russian Academy of Sciences

REVIEWS OF TOPICAL PROBLEMS

PACS numbers: **61.48. – c,** 79.20.Eb, **81.07. – b**

40th ANNIVERSARY OF THE PROKHOROV GENERAL PHYSICS INSTITUTE, RUSSIAN ACADEMY OF SCIENCES

Electrophysics of carbon 1D structures obtained in a laser experiment: models and demonstration

S V Garnov, D V Abramov, D N Bukharov, T A Khudaiberganov, K S Khor'kov, A V Osipov, S V Zhirnova, A O Kucherik, S M Arakelyan

DOI: https://doi.org/10.3367/UFNe.2023.12.039620

Contents

Abstract. Laser-induced carbon 1D structures and some of their electrophysical properties have been studied by means of computer simulations. Evidence of the possible emergence of a new allotropic phase of carbon (carbyne) produced through laser melting of graphite has been experimentally demonstrated. Methods for obtaining topological nanoclusters of controlled modifications using laser ablation are discussed, and the obtained images are presented. The main results of modeling 1D structures with fractal fragments are considered. Raman spectra with corresponding confirmation of the existence of laser-induced low-dimensional carbon structures are displayed. The structures discovered enable the development of next-generation elements and devices for nanoelectronics and nanophotonics based on new physical principles.

S V Garnov [(1)], **D V Abramov** [(2, *)], **D N Bukharov** [(2)], **T A Khudaiberganov** [(2)], **K S Khor'kov** [(2)], **A V Osipov** [(2)], **S V Zhirnova** [(2)], **A O Kucherik** [(2)], **S M Arakelyan** [(2)]

[(1)] Prokhorov General Physics Institute, Russian Academy of Sciences, ul. Vavilova 38, 119991 Moscow, Russian Federation

[(2)] Vladimir State University named after Alexander and Nikolay Stoletov, ul. Gorkogo 87, 600000 Vladimir, Russian Federation

E-mail: [(*)] awraam@mail.ru

Received 8 September 2023, revised 4 December 2023
Uspekhi Fizicheskikh Nauk **194** (2) 115 – 137 (2024)
Translated by M Zh Shmatikov

Keywords: 1D structures, laser melting of graphite, carbyne, laser ablation, modeling of fractal objects, 1D electrophysics, experimental demonstration

1. Introduction

The existence of allotropic forms of carbon and their formation, properties, and applications have been explored for more than a decade, which is explained by the unique properties of various configurations of carbon atoms and metal-carbon complexes. The development of laser technology makes it possible to create new conditions for the formation of various carbon micro- and nanostructures, ranging from carbyne to diamond.

Indeed, the use of laser ablation of materials in a liquid (see, for example, [1]) enables realization under normal ambient conditions of extreme conditions in local areas even when they are exposed to relatively low-power laser radiation. This leads to a number of conceptual phenomena, in particular, first, to the formation of completely thermodynamically stable micro- and nanodiamonds from a graphite target in a liquid as a result of nonequilibrium phase transitions [1], and, second, to the emergence of a special allotropic form of carbon, carbyne (see, for example, experiments [2–5]) with 1D-carbon chains. The obtainment of such long 1D chains, Long Linear Carbon Chains (LLCCs), is now a routine process within a certain procedure of laser ablation of carbon materials in association with noble metals (see, for example, [6–10]). Although other methods for carbyne synthesis are available (see, for example,

[6, 9, 11, 12]), it is laser schemes that are the most promising in terms of controlling these processes, exploring their physical nature, and predictive modeling of their parameters. In principle, carbyne is understood as a system consisting of only carbon chains that can be packed into crystals due to van der Waals forces. The synthesized chains are assumed to be rectilinear, since each electronic state of the C atom is described by sp-hybrid wave functions [11]. However, different structures with angular kinks also arise, which determine their functional characteristics. Such systems can self-organize into certain ensembles.

The electrophysical properties of systems with various spatial dimensions (from 0D to 3D) are governed by symmetry factors and their modification under conditions of topological phase transitions into various electronic states, depending on the shape, size, and spatial distribution of such objects, usually on the surface of a solid body (see, for example, [12]). It sometimes occurs with abnormal characteristics. For example, depending on topological parameters alone, electrical conductivity can increase in thin films by several orders of magnitude (compare, for example, with [3]).

Recently, such systems have been intensively studied in terms of 'unusual' crystalline/metallic structures [13] and other nonstandard objects [14].

Of particular interest here are 1D systems formed in various configurations, which, due to a large dipole moment and high electrical polarizability in a single preferred direction, can feature unusual electrophysical characteristics. Here, it becomes possible to study the tendency to attain a superconducting state (see, for example, [15]). The effective masses of electrons and holes and the band gap in such systems strongly depend on the topology of the emerging low-dimensional structure. Therefore, such fixed key parameters of materials, including the Fermi level, can be significantly modified.

In this regard, it is carbon (C) compounds that are of great importance, including their combinations, as already noted, with noble metals, in particular, when LLCCs are fixed between noble metal atoms at the edges of the chain, for example, two gold (Au) and/or silver (Ag) atoms. Such structures are stable. Systems with high electrical polarizability arise especially effectively when the sizes of these metal-containing objects (for example, nanoparticles) at the LLCC edges are different. The formation of such LLCCs can be easily observed, for instance, using Raman spectroscopy both in a colloid and in thin films on a substrate with deposited LLCCs. Carbyne itself features n-type semiconductor properties; under the influence of light, its electrical conductivity increases, and such photoconductivity, induced by even low-power laser radiation, is easily observed.

A separate issue is the creation of metasurfaces based on such LLCCs (sp-electron configuration) [16] when they are deposited on the surface of a solid substrate, including by the method of a spraying jet [6 ,17].

All this refers to real phase transitions [18–21] to a new allotropic form of carbon, carbyne, obtained, for example, by us using various laser experiment techniques [4, 5, 10], which can be joined in various configurations.

In this case, both cumulene bonds $(=C=C=C=)_n$ with a binding energy of 0.41 eV and polyyne bonds $(-C\equiv C-)_n$ with a binding energy of 1 eV, stabilized by the 1D structure, in our case, by noble metal atoms at their ends, can emerge. For practical tasks of controlling the functional characteristics of various systems, such objects are especially important when they can be additionally orientated in space in external fields (cf. [22]).

Quantum phenomena of electrical conductivity in such systems are manifested when the de Broglie wavelength λ_{dB}, which determines the coherent length, exceeds the characteristic spatial scale (Λ) of the system (see, for example, [23, 24]). This condition $\lambda_{dB} \gtrsim \Lambda$ for a linear carbon structure, which can be easily realized, leads to the suppression of electron–phonon scattering on this scale with a strong increase in the electrical conductivity of the entire structure containing LLCC objects. This effect is exhibited even if the structure deviates from strict linear ordering in individual sections, but provided that their lengths are less than λ_{dB} (for carbon, its value can be of the order of several ten nanometers, in contrast to metals with $\lambda_{dB} \sim 1$ nm) [25]. Therefore, modeling various types of such fragmentary deviations from the overall dominant linear direction with the presence of fractal objects (segments) of arbitrary orientation is of particular interest in terms of their association in various topological structures.

In our experiments [10, 26], we obtained a sharp nonlinear increase (by tens of times) in the electric current in the (Au–C–Au) compound compared to the value that follows from the usual Ohm's law for a standard conductive system: in a thin film 30 nm thick for an applied external voltage of 1.5 V, the current strength was 0.5 A. Such an object containing an LLCC was synthesized in a two-stage laser experiment (see, for example, [4]). First, a shungite sample was subjected to laser ablation and a colloidal system with nanoobjects was obtained, and next laser deposition from the colloid onto a solid substrate was used (taking into account fragmentation effects). The formation of LLCC objects was monitored using luminescence spectra and Raman scattering. In these experiments, a 4D technology of the synthesis of such objects was actually implemented. Namely, in addition to three spatial parameters of the laser-induced object, the fourth parameter was also of fundamental importance: it is the time associated with both the fixation in the experiment of the duration of irradiation of the system and the selected duration of the exposure to laser radiation [4, 5, 10, 25] (cf. [18]).

In this case, for example, for femtosecond light pulses, certain nonequilibrium phase transitions occur with a nonstationary formation of structures of various dimensionality [8, 10, 18, 27, 28].

An important feature of such one-dimensional systems is also the nonmonotonic behavior of the resulting current-voltage dependences exhibiting jumps of electrical conductivity in certain cases (for example, analyzed using the simple Kronig–Penney model), including analogues of Fano resonance [23, 24]. In [29–31], we actually obtained a model implementation of such regimes.

Here, various qualitatively different states can arise, depending on dynamic processes for one-dimensional chains, for example, as a result of their self-intersection involving the formation of nontrivial loops with the manifestation of interference [16–24] and other effects [32], such as Wannier–Stark ladder electrical conductivity, Mott's law with a Coulomb blockade, and the manifestation of quantum laws [23, 24, 33, 34]. Of special interest are quasiparticles in systems with a certain microcavity-type spatial periodicity, which are now actively being studied in plasmonics, polaritonics, and spintronics (cf. [29, 30, 35, 36]). However, we skip the optical characteristics of such complex structures with

their control in a given direction, although this is one of the most essential areas of modern photonics. The presence of surface electromagnetic waves is the main reason for the formation of various types of surface periodic structures as a result of the interference among the incident radiation wave, surface waves, and waves scattered (diffracted) due to the inhomogeneity of the surface material.

We consider here a number of problems from the list of those presented above, both in theory and in laser experiments, and in the corresponding models. We focus on progress in the area of one-dimensional carbon complexes obtained by various methods with corresponding interpretations of the problems arising there, which are widely discussed in this field of knowledge [37–52].

Section 2 is devoted to methods for obtaining topological ensembles of nanocluster 1D-carbon structures in laser experiments using laser ablation. Their configurations are analyzed based on the measured optical spectra of various types. In Section 3, the main results obtained in electrophysics are discussed and interpreted, taking into account the modeling of 1D structures with fractal segments oriented in different directions; other electrophysical characteristics of 1D structures are also considered. Section 4 presents general integral spectral measurements for 1D structures in carbon complexes affected by laser radiation. In Section 5, the results obtained are considered in relation to the key priorities in modern research on this topic, in both basic and applied physics.

2. Methods and experimental conditions. Laser-induced structural phase states

2.1 Methods and approaches: experimental demonstrations

Given the availability of powerful laser pulses with an energy sufficient to break crystalline bonds in a system during their interaction with the surface of the irradiated sample, nanosized particles can be synthesized from almost any solid material. The laser ablation experiment does not involve any restrictions characteristic of explosive and chemical methods for creating nanoscale structures, since the main parameters governing the dynamics of laser radiation interaction with matter, which is a tool for affecting an object, are only the absorption spectrum of electromagnetic radiation and the thermal conductivity coefficient. Both of these parameters can be taken into account in a laser experiment, and, when using laser sources with various radiation wavelengths and pulse repetition rates, by varying the applied power, focusing, and scanning mode of the laser beam over the sample surface, such experimental parameters can be selected that satisfy the conditions for ablation of the overwhelming majority of materials. This is the basis of the approach to obtaining carbyne in our case.

Figure 1 shows the well-known phase diagram for the region of the existence of carbyne, proposed in classical work [42], which some time ago was the subject of lively debate (see, for example, [11, 44]). Currently, this concept is generally recognized. For laser experiment, the brightness temperature of melting of glassy carbon measured during heating is 2720 K (see [3]), a value which is consistent with the displayed diagram for the region where carbyne exists.

In our method, we obtained 1D-carbon structures by laser ablation of a carbon target in a liquid, followed by the deposition of carbon complexes from the resulting colloidal system onto a solid substrate.

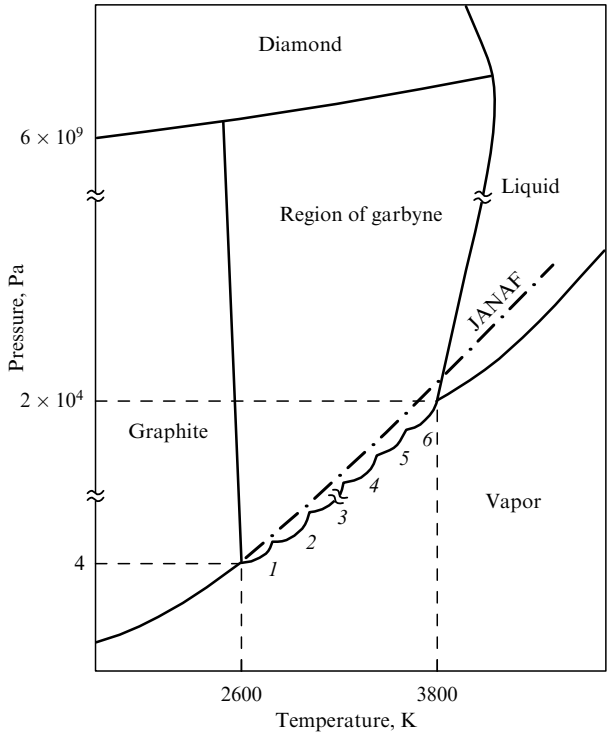

Figure 1. Phase diagram of carbon. Numbers *1–6* mark the stability ranges of the six carbyne forms identified by the author of [42]. Dashed lines mark the graphite–carbyne–vapor and carbyne–liquid–vapor triple points on the phase diagram.

This technique was selected because the impact of pulsed lasers on a target is especially suitable for creating nonequilibrium conditions due to the short time scale of temperature change. Local laser-induced evaporation leads to the occurrence of extremely high temperatures at which carbon particles transform during the experiment into carbon vapors, and, in the presence of a catalytic additive (noble metal nanoparticles), di-/trivalent carbon–metal compounds can be synthesized.

Thus, the main advantages of laser synthesis of nanoparticles are the controllability of the laser experiment, the dynamic response of the exposure medium, and the implementation of an active interphase transition. With an appropriate choice of laser radiation wavelength and target material, high radiation energy densities are absorbed by a small volume of material, and local evaporation occurs. It is this effect that leads to a controlled synthesis with controllable composition of the films subsequently obtained from the ablated material on a solid surface.

Various possible configurations of self-organizing carbon objects — sponge structures obtained in the presence of gold nanoparticles (Au) in the laser experiment setup we used (Fig. 2a) — are shown in Fig. 2b–d. The images were obtained using various registration techniques: high-resolution transmission electron microscopy (TEM image) and scanning electron microscopy (SEM image).

Figure 3 displays the modification of Raman spectra of carbon linear structures obtained by us in a colloid, depending on their configuration (cf. [16, 25]).

Thus, even if 1D objects are present as pieces, they can be joined in ensembles of various types. Therefore, it is of importance to have available methods for actually synthesizing/fixing such carbyne elements in the form of chain objects,

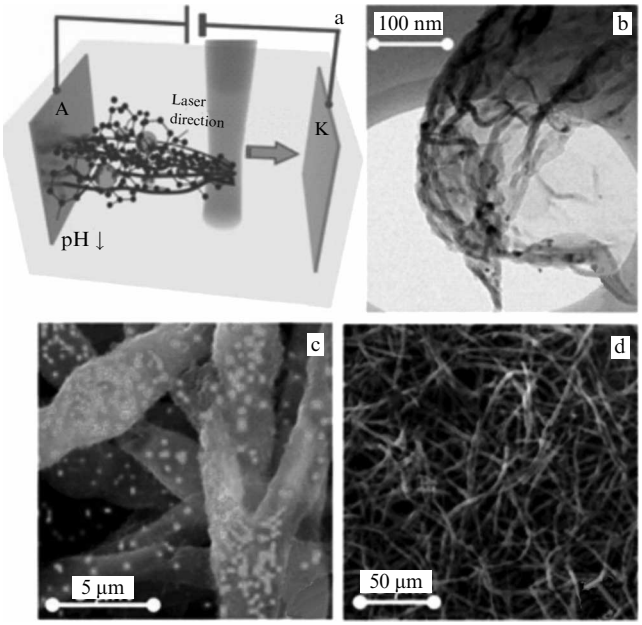

Figure 2. (a) Geometry and conceptual layout of self-assembly of spongy structures based on sp^2 carbon doped with a high concentration of sp-carbon bonds. (b) TEM image of a fragmentary part of a cleaned sponge (dark dots correspond to Au nanoparticles). (c) SEM image of spongy structures combined with the results of EDAX elemental analysis that show the accumulation of nanoparticles at the centers of segments and splitters of each cluster (distribution of gold is shown with light spots). (d) Full map of the resulting structures at the macroscale.

especially on solid substrates when they can be potentially used in elements of micro- and nanoelectronics and photonics.

We discuss below an experiment on laser fragmentation of colloidal systems consisting of amorphous carbon, which was also carried out under the conditions of a constant external electric field of low intensity (voltage of 12 V at a distance between electrode microcontacts of 3 mm) and/or magnetic field applied. A strong polarization of the resulting carbon molecules was observed, which led to the formation of extended 1D filaments when they were deposited on the substrate. Although these structures were coils of filaments rather than isolated filaments, their predominant growth (1D structure) in a single direction along the field was nevertheless evident. We have simulated such a process of geometric nematicity in the approximation not of a gaseous atomic carbon system but of an ensemble of formed C_2 and C_4 molecules, i.e., when two or four carbon atoms are included in a single linear molecular structure, which is confirmed by measurements of luminescence and Raman spectra. The spectra of final carbon structures have maxima characteristic of objects with carbon chain lengths varying from 8 to 24 carbon atoms; they were detected using a transmission electron microscope. This is a fairly good result in the synthesis of chain carbon.

It should also be noted that the effect of nematicity violation — deviation from the linear structure in various fragments, which is often observed in linear structures of carbon and was also modeled by us (see Section 3.1) — is a basic symmetry factor and can lead, notably, to a significant increase in electrical conductivity due to topological features and boundary phenomena in such systems [37–40]. An analogue of this phenomenon is also considered below.

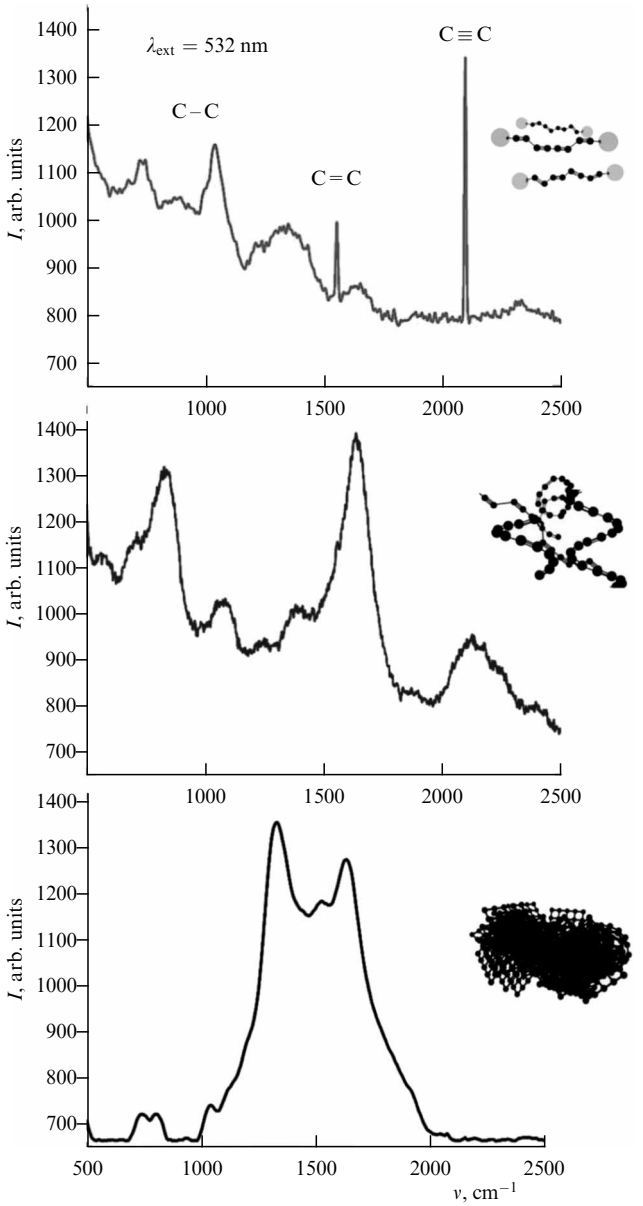

Figure 3. Raman spectra in colloidal systems with various configurations of carbon structures. Noble metal atoms located at the ends of the chain are indicated in the upper part. Excitation wavelength λ_{ext} = 532 nm.

2.2 Experimental measurement techniques

Methods for controlling the topology of objects on a sample surface in processing carbon targets with laser radiation in a laser ablation setup. The controlled formation of topological nanoclusters in multilayer thin films on the surface of a solid body was realized in our experiment using two-stage laser methods (see, for example, [4, 25]).

First, nanoparticles/nanoclusters were synthesized in the process of laser ablation of targets made of various materials placed in liquids to obtain a colloidal system. Laser radiation was used with various pulse durations with a repetition frequency of 20–100 kHz, pulse duration ranging from milliseconds to femtoseconds, and an average power density on the target of $10^6 - 10^7$ W cm^{-2}.

At the second stage, nanostructures were deposited from the colloid onto the surface of a solid substrate under the influence of continuous laser radiation of various powers (up to 10 W) while implementing a certain strategy for scanning

Table. Laser system parameters.

Radiation wavelength, nm	1030
Pulse repetition frequency, kHz	10
Pulse duration, fs	280
Beam diameter, mm	4.5
Pulse energy, μJ	153

the colloidal system with the laser beam. This made it possible to obtain a nanostructured system with a given topology on the surface of a solid substrate. In obtaining 1D structures, external electric/magnetic fields were also applied to enhance the orientation of nano-objects in selected directions.

To obtain various configurations of carbon structures, including graphene layers, a femtosecond Yb:KGW laser system was used as a radiation source. The main parameters of laser radiation employed for a glassy carbon target are presented in the table.

This made it possible to obtain average radiation powers on the irradiated target ranging from 100 to 1000 mW. A glassy carbon target was exposed to femtosecond laser radiation along a trajectory in the form of successive parallel dashed lines along the surface of the sample with various processing modes. Twenty-five areas were made in the form of squares, one mode per square. The modes differed in the laser radiation power. Xylene, a liquid hydrocarbon which consists of a benzene ring and two methyl groups, was used as an auxiliary liquid to obtain a colloid in the femtosecond experiment. Its chemical formula is $(CH_3)_2C_6H_4$. The height of the liquid layer above the target surface was usually 1 mm.

In the resulting colloid, with continued exposure to femtosecond laser radiation, fragmentation and/or clustering of nanostructures occurs, depending on the irradiation modes (cf. [41]).

Procedure for measuring electrical properties. This section presents the technique for measuring the current-voltage characteristics of the nanocluster/island nanofilm samples we obtained. The analysis was carried out using the well-known four-probe scheme with a linear arrangement of microcontacts at points on the surface [10, 25]. Two outer contacts, which provided a DC supply using a stabilized power source, were located at a fixed distance from each other. Inner probes, which could move along the surface, were conductive needles of an atomic-force microscope with a curvature radius of 100 nm. This setup made it possible to carry out measurements at various selected distances between these probes. The probe pressing force was about 1 N. The required current was set at the power source, and the corresponding voltage was measured by a voltmeter. To carry out temperature measurements, the entire circuit was assembled in a vacuum thermal chamber which could be pumped out to 10^{-3} Torr, and the sample could be heated to 100 °C.

2.3 Ensembles of linear-chain carbon structures and conditions for the appearance of various carbon configurations with certain phase states in a laser experiment

Omitting the history of the investigation of phase diagrams of carbon with the prediction of its allotropic stable linear-chain sp-hybridized phase, carbyne, in the temperature range of 2600–3800 K (see one of the first papers already mentioned [42] and Fig. 1) with a triple point at a pressure of 2×10^4 Pa and a temperature of 3800 K, we note that it was determined in our study [2] that, in the process of heating and melting carbon samples, the heating rate is of fundamental importance, and carbyne appears if its value at the specified temperature mode is less than 10^2 K s^{-1}. In the case of laser heating, this parameter is controlled by the duration of the laser pulse and its focusing when processing the target, which leads to the melting of carbon at atmospheric pressure.

We observed such melting for the first time in real time using an appropriate laser circuit for monitoring and controlling the dynamic process (using a brightness amplifier based on a copper vapor laser source to obtain images) [43]. This technique made it possible to directly observe the melting and flow of liquid carbon with further study of the evolution of the structure of graphite remelted in this way using atomic force microscopy in tunnel scanning mode (compare with a model of the atomic structure of liquid carbon [38]).

The Raman spectra recorded using a cooled CCD detector actually showed that, along with the D (disorder) and G (graphite) lines characteristic of graphite and equal, respectively, to ≈ 1333 and ≈ 1581 cm^{-1}, melting (at a temperature no higher than 4000 °C) was unambiguously detected in certain areas of the surface of the sample of the chemically pure graphite used, which was, however, strongly disordered initially and subjected to laser exposure. In the melting zone, the emergence of a carbyne phase was observed, which was detected by Raman spectra in the spectral region of ~ 2000 cm^{-1}. This demonstration, which we reliably confirmed, was recorded in subsequent experiments (see, for example, [4, 5]). The degree of ordering (homogeneity) in the zones of such laser exposure indicates the completed process of laser melting and formation of the liquid phase of carbon which was removed to a distance of 0.2 mm in a time of 0.3 s, a laser spot being spatially anisotropic in the form of an irregular ellipse with major axes of about 0.15 and 0.7 mm (observed using an optical microscope).

Concurrently, we experimentally studied laser-induced processes on the surface of carbon-containing materials (in particular, glassy carbon and pyrocarbon) with simultaneous measurement of its brightness temperature (T_r) using a high-temperature pyrometer. In these measurements, the brightness temperature of glassy carbon was $T_r = 2720 \pm 15$ K (see [3]). This value corresponds to the true melting temperature (T) under actual experimental conditions of the order of 3300 K in accordance with the relation

$$\frac{1}{T_r} - \frac{1}{T} = \left(\frac{\lambda}{c_2}\right) \ln\left(\frac{1}{\varepsilon_{\lambda,T}}\right),$$

where λ is the wavelength (1070 nm), $c_2 = 0.01488$ mK, and $\varepsilon_{\lambda,T} = 0.73$ is the emissivity of the surface, taken from reference book [122].

In what regards the electrophysical characteristics with the charge transport properties of carbyne, LLCC can be consolidated into various configurations of topological micro- and nanostructures of linear carbon chains in thin films (see, for example, [38, 45, 46]). This consolidation is accompanied by phase transitions of various types, for example, conductor–insulator, and even by a tendency based on the physical mechanism of electron pairing to a superconductivity state with a certain size and arrangement of nanoclusters (cf. [15]) and to states featuring photoconductivity and ferromagnetism (cf. [47–51]). The physics of such

phenomena are associated with specific boundary forms of the band gap, the corresponding Fermi level, and their relative position determined, in particular, by the topology of nanostructures (similar to the role of donor-acceptor impurities in a bulk semiconductor sample). In our case, it is related to various configurations of metal-carbon and other compounds, including inhomogeneous and disordered structures, and, therefore, to a low value of the electron work function (~ 0.1 eV), in particular, based on the mechanism of thermal emission through changing parameters of contact energy barriers and potential wells (cf. [52–55]).

Physical processes and their time diagrams in the realized sequence of phenomena occurring during the interaction of pulsed laser radiation for various laser pulse durations have been analyzed in [56–58]. Laser ablation with melting and modification of the surface morphology in local samples usually occurs if nano- and picosecond laser pulses are used.

Femtosecond laser experiment. When a target placed in various liquids is irradiated with femtosecond laser radiation, local ultra-fast heating of the target occurs, due to which heat removal in the material is very weak. The main ablative effects are associated then with the regimes of evaporation, hydrodynamic expansion (phase explosion), and separation of part of the layer during melting into the bulk of the sample under conditions of subsurface boiling and foam formation at certain temperature gradients. For carbon targets, various allotropic forms of carbon can be obtained by combining sp-, sp^2-, and sp^3-hybridized carbon atoms, including sp^2 graphene ribbons. Then, configurations with different dimensional structures may arise, which are usually classified for stable phases as follows: 0D — carbon point; 1D — carbon chains and nanotubes; 2D — graphene, multilayer graphene sheets; 3D — fullerenes, graphite, and diamond [59, 60]. However, metastable phases can also be synthesized, for example, micro- and nanocubes of monocrystalline carbon with a body-centered cubic structure with a fixed lattice constant of 5.46 Å [61].

The 1D structure in the form of the allotropic structure of carbon we are considering, such as carbyne [9, 11, 42, 44], actually develops if simple and inexpensive ablation methods are applied [4, 5, 10]. All these structures can be joined into various low-dimensional twisted spatial structures containing, for instance, different types of graphene objects (cf. [19, 20, 22]).

Figure 4 shows the graphene ribbons and plates we obtained, torn off from a target of highly oriented pyrolytic graphite and a glassy carbon sample and placed in liquid nitrogen under the effect of femtosecond laser radiation. The mechanism of graphene formation in liquid nitrogen is associated with nitrogen penetration into the interlayer distance of the graphite lattice [62].

Figure 5 presents Raman spectra for various numbers of graphene layers formed as a result of such effects.

We also recorded the formation of extended periodic nanostructures on the surface of carbon samples and various forms of carbon crystalline structures, including nano- and microdiamonds [10, 26].

In the former case, during laser irradiation of the surface of carbon samples, the appearance of such specific laser-induced periodic surface 1D nanostructures, 'ripples,' is associated with interference between incident pulses of precisely femtosecond duration and the light scattered from defects on the surface of the sample (cf. [63]).

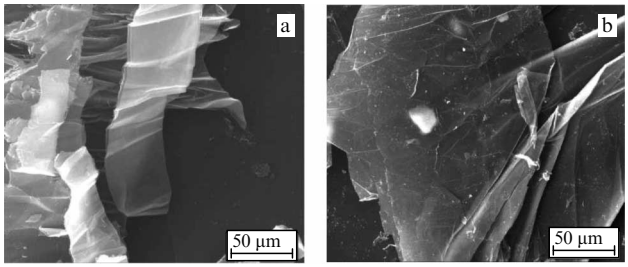

Figure 4. Graphene ribbons (a) and plates (b) split off from the main sample under the effect of femtosecond laser radiation on highly oriented pyrographite in liquid nitrogen.

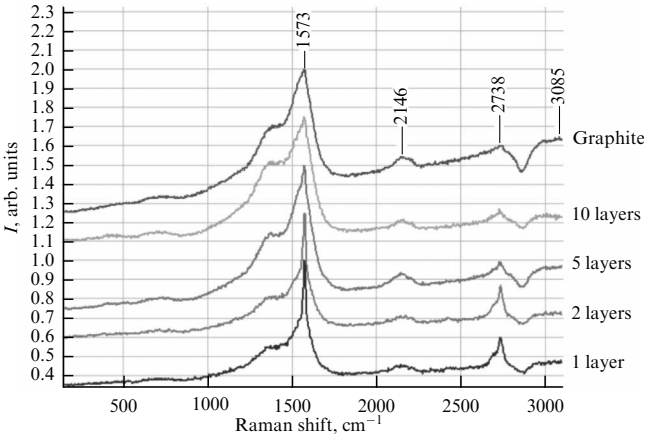

Figure 5. Raman spectra of the graphene formation region under laser irradiation of a pyrographite sample placed in liquid nitrogen: number of graphene layers is indicated on the right.

The formation of crystalline structures is driven by inhomogeneous and unsteady heating of the surface of the material and parts of the melt penetrating into the liquid low-temperature medium (cf. [1]).

We have found that such systems are especially clearly manifested under laser action on a target in air when the surface of samples is scanned with a laser beam at a speed of the order of 10 mm s^{-1}.

Suchlike structures may provide an option for the development of inexpensive nanoelectronic devices of the next generation of printed electronics in the form of high-quality carbon nanogrids (cf. [55]).

1D-carbon structures and their identification in interpreting spectral measurements. To synthesize linear carbon chains in liquid, we used the method of laser fragmentation of colloidal carbon systems, which enables obtainment of stabilized carbon chains. To create carbon–gold bonds in a colloidal solution to stabilize the chain structure, the sample was additionally irradiated with nanosecond laser pulses generated by an ytterbium (Yb) fiber laser with a central wavelength of 1.06 μm, pulse duration of 100 ns, repetition rate of 20 kHz, and pulse energy up to 1 J. The time between subsequent pulses was about 1 s. The dimensions of gold nanoparticles were controlled using a Horiba SZ100 dynamic laser scattering device. The formation of the polyyne carbon phase ($-C \equiv C-$) was recorded based on Raman spectra measured using a Senterra spectrometer (manufactured by Bruker, USA). The pump laser wavelength in this device was 532 nm at a power of 40 mW; the radiation was focused through a 50x microlens; and the spectra were recorded in a confocal microscope configuration and averaged over

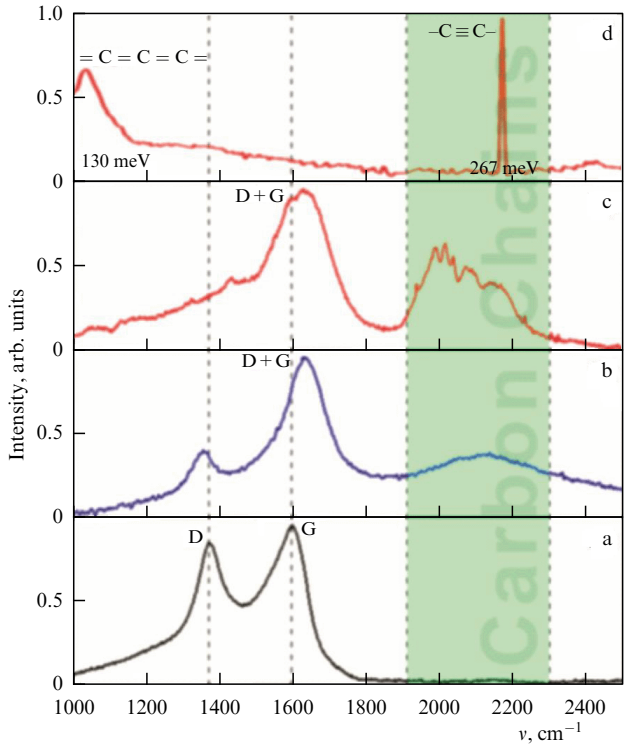

Figure 6. Measured Raman spectra of a colloidal solution at different stages of the LLCC laser synthesis process. (a) Raman spectrum of the original shungite in liquid (lines D and G). (b) Spectrum of unstabilized carbon filaments in solution (D+G). (c) Transformation of spectra at beginning of the appearance of carbon chains synthesized in the presence of gold nanoparticles. (d) Characteristic vibration modes of isolated linear chains for polyyne (−C ≡ C−) and cumulene (= C = C = C =) bonds. Vertical shaded band is the spectral region for carbyne (LLCC band).

10 measurements. The accumulation time of each measurement was 60 s.

To examine in detail the orientation distribution of 1D nanodipoles of carbon, studies were carried out by means of high-resolution transmission electron microscopy and X-ray diffraction analysis using FEI Titan3 with a spatial resolution of up to 2 Å. TEM images and diffraction patterns were processed using the open database package Image J 1.52a.

We present below some characteristic features of our measurements.

First. Resonance Raman spectroscopy was used to identify the synthesis of LLCCs with their quantitative yield at different stages of synthesis. Raman scattering bands are interpreted as degradation of the defect-induced (D-band) and graphite (G-band) modes during laser exposure (see, for example, [4]). The presence of LLCCs exhibits an active Raman scattering mode in the so-called LLCC band. Polyynes with less than 20 carbon atoms are characterized by bands located between 1900 and 2300 cm^{-1}. The resulting spectra corresponding to LLCCs with gold atoms/nanoparticles are shown in Fig. 6.

The obtained Raman spectrum of a colloidal solution containing carbon chains stabilized with gold is represented by the upper red curve in Fig. 6. The peaks correspond to the characteristic vibronic modes of the polyyne allotrope. No signals characteristic of stretching modes of the carbon chain are observed. Traces of the D- and G-bands are completely blurred in the spectrum displayed in the upper panel of Fig. 6, where only strong peaks characteristic of polyyne chains are visible. This is confirmation that our experiments indeed revealed the predominance of the sp-carbon phase in the colloid.

Second. Photoluminescence (PL) of carbon chains (Fig. 7) was detected using a pulsed Ti:Sapphire laser system (Coherent Chameleon Ultra II) with a central wavelength of 800 nm, a pulse duration of 140 fs, and a repetition rate of 80 MHz, pumping an optical parametric oscillator, which allows precise control of the excitation energy. As a result, three different excitation wavelengths were used to clarify the nature of the fine lines observed in the PL spectra, namely, 390, 380, and 370 nm, as shown in Fig. 7b. The exciting radiation was focused on the sample using a Mitutoyo M Plan APO SL 50x microscope lens with a numerical aperture of 0.42. Since the sample was installed in a Montana Instruments Cryostation C2 closed-cycle cryostation, PL measurements were carried out in a vacuum in the temperature range of 4–300 K. Without going into experimental details, we only note that the PL signal was recorded by a Princeton Instruments SP2750 spectrometer with a spectral resolution of 0.1 nm. Several distinct peaks were observed in the sample PL, corresponding to optical transitions of carbon chains of various lengths. Furthermore, during a spectroscopic analysis of the PL dynamics associated with identified optical transitions, using counts of single photons with their time correlation (the so-called TCSPC method), it was possible to

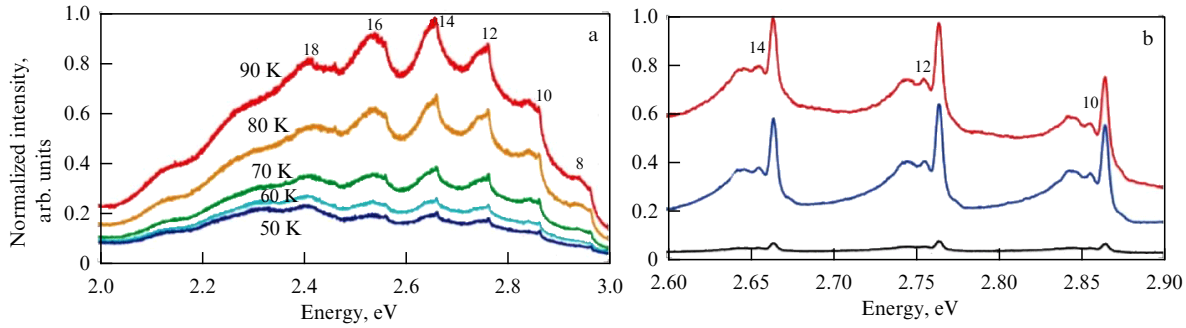

Figure 7. PL spectra (in units of eV) of applied polyyne chains of various lengths (number of carbon atoms in the chain is indicated above corresponding spectral resonance). (a) Spectra obtained at temperatures from 90 to 50 K (red curve corresponds to 90 K; yellow curve, to 80 K; green curve, to 70 K; turquoise curve, to 60 K; and blue curve, to 50 K). Laser excitation wavelength is 390 nm; intensity is 5 mW; and recording time is 10 s. (b) PL spectra recorded at 4 K. Red, blue, and black curves correspond to excitation wavelengths of 390, 380, and 370 nm, respectively, obtained using a parametric light generator. Measurement time is 40 s.

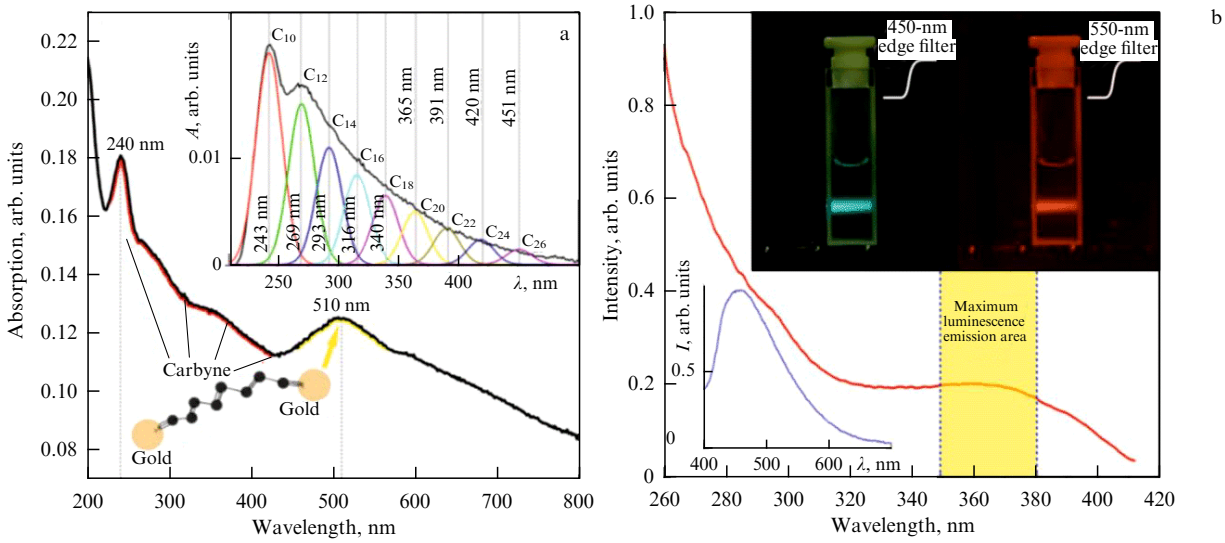

Figure 8. (a) Absorption spectra of carbyne chains stabilized by gold nanoparticles in a colloidal solution; inset at the top shows model dependences (Gaussian curves) with the exponential background characteristic of the main absorption band subtracted. In this way, a sequence of resonances is detected, the envelope of which yields the integral absorption spectrum. (b) Spectra upon excitation of photoluminescence (blue line) and emission of photoluminescence itself (red line) of the colloidal solution. Region of maximum luminescence emission is also marked.

record PL spectra with the identification of spectral lines within the 5-nm line width, which corresponds to exciton and trion transitions (cf. [24]).

Third. Additional information about the structural properties of the synthesized carbon chains is provided by the optical spectra of photoluminescence excitation, which we recorded using a Horiba Fluorolog-3 spectrofluorimeter with a spectral resolution of 8 nm. The pump wavelength for detecting the photoluminescence signal was fixed at a maximum of 442 nm, and the recorded photoluminescence wavelength varied from 260 to 430 nm.

The absorption spectra of solutions containing carbon chains (Fig. 8a) exhibit a characteristic absorption band of carbon in the wavelength range of 240–350 nm and a band corresponding to the plasmonic absorption of gold nanoparticles (about 510 nm), which is shown by the yellow arrow from the atom of gold. The inset to Fig. 8a shows that the strongest absorption is observed in the spectral range near 240 nm. This band corresponds to the absorption of light by linear carbon chains containing 10 atoms [64]. Local absorption maxima are also observed in the spectral range of 240–450 nm, characteristic of linear chains of C10–C26 carbon atoms. These peaks, which can be fitted by Gaussian functions, are also shown in the inset to Fig. 8a.

Photoluminescence of carbynes in a colloidal solution (blue line in Fig. 8b) was excited by the third harmonic (355 nm) of a neodymium laser and recorded through spectral filters at the edges of the 450–550-nm band. The right inset to Fig. 8b displays photographic images of the luminescent solution taken with these 450- and 550-nm filters, which suppress the light scattered from the laser (red curve in Fig. 8b).

An enhancement of the photoluminescence signal was recorded at wavelengths of 350–380 nm. This is typical of the excitation of photoluminescence via electronic transitions between the highest occupied molecular orbital (HOMO) and the lowest unoccupied molecular orbital (LUMO) for the valence and conduction bands, respectively, with subsequent recombination during pumping with $\lambda = 442$ nm (cf. [65, 66]). The photoluminescence spectrum of the colloidal solution (blue line in Fig. 8b) indicates that the HOMO–LUMO splitting (band gap) in the synthesized system containing carbyne varies in the range of 400–600 nm (peak in dependence in Fig. 8a). The width of the energy gap with linear carbon chains is also sensitive to the length of the 1D chain itself. Quenching of photoluminescence in a colloidal system prevents the observation of resonances that appear in absorption spectra (Fig. 8a). On the other hand, this provides an estimated HOMO–LUMO splitting of 2.9 eV or higher, which is consistent with calculated predictions for a carbon chain of 8–16 atoms [20]. Interpretation of the absorption spectra (inset to Fig. 8a) shows that the most common carbon chains contain 10 atoms, but some chains reach a maximum length of 26 atoms.

Fourth. To deposit carbon chains stabilized by gold atoms onto a solid substrate (fused quartz glass), drops of a colloidal solution were applied and dried. In such objects containing carbon chains stabilized by gold nanoparticles, anchors, the 1D orientation persisted in certain areas. Figure 9a shows the excitation of photoluminescence, again using radiation at a wavelength of 442 nm, along with the spectrum of photoluminescence excited at a wavelength of 370 nm (inset to Fig. 9a). The spectra are characteristic of molecular systems: they overlap, and Levshin mirror symmetry with respect to the dip between values of 370 and 442 nm is clearly observed (cf. [20]). The Stokes shift of photoluminescence relative to the pump, caused by nonradiative relaxation processes, is about 4400 cm^{-1} between the two maxima in the curves.

According to Pan et al. [20], the emission maxima (photoluminescence) of the spectrum components shown in Fig. 9a at 410, 435, and 465 nm, correspond to HOMO–LUMO transitions in carbon chains consisting of 8, 10, and 12 atoms, respectively. Following the approach of [20], we approximated the observed broad photoluminescence band by a set of Gaussian peaks corresponding to various lengths of carbon chains. The broadening of all Gaussian peaks was considered equal to reduce the number of free model parameters. This analysis made it possible to construct a

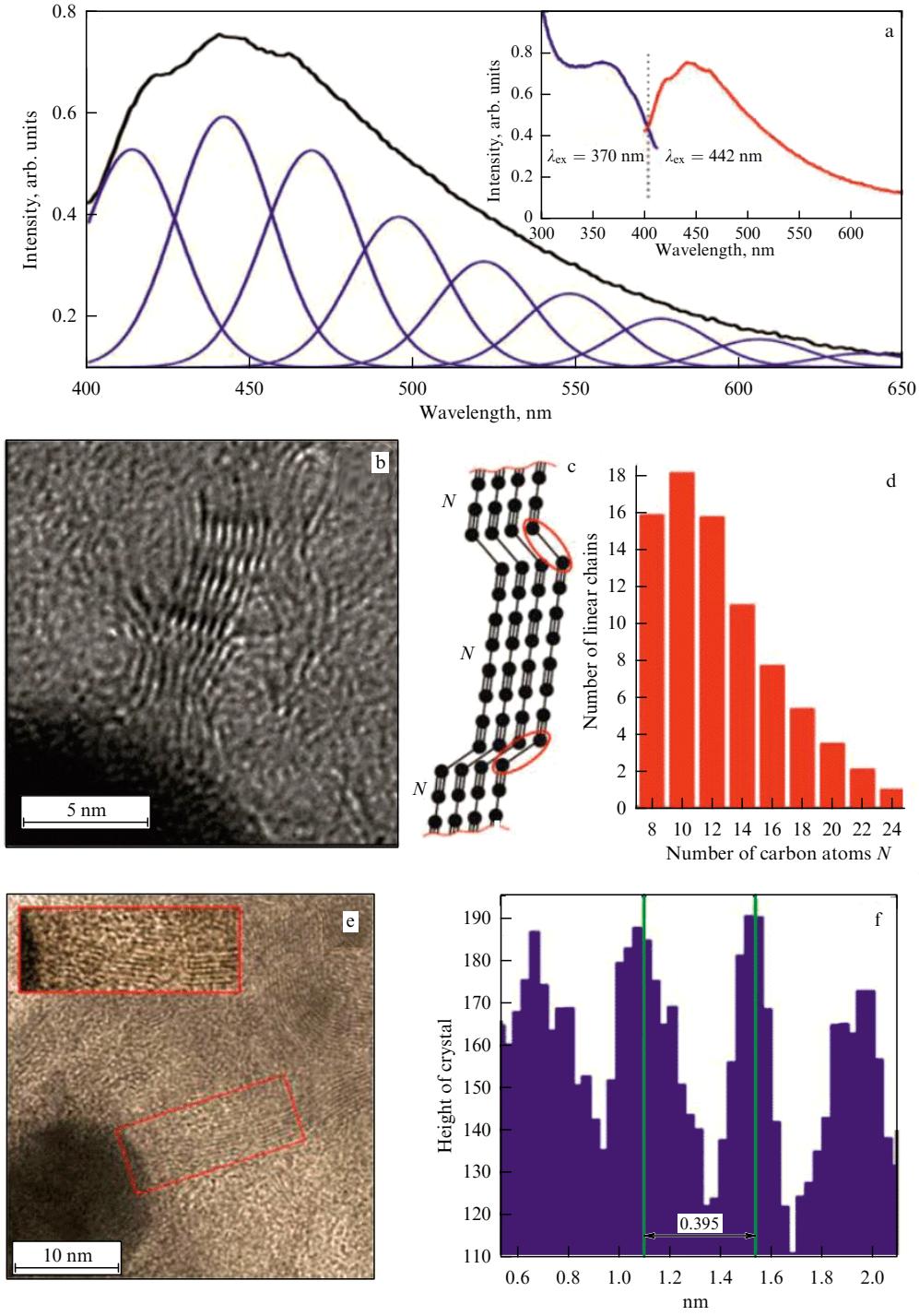

Figure 9. (a) Photoluminescence spectrum of a carbyne film on a substrate made of fused quartz glass (black line) and approximation of its components by the distribution of Gaussian functions corresponding to individual carbon chains (with different number of C atoms (cf. Fig. 8a)). Inset shows photoluminescence spectra upon excitation by pumping at $\lambda = 442$ and 370 nm (blue and red lines, respectively) for carbynes deposited on the substrate. (b) TEM image of the carbyne film under study; an ensemble of 1D-carbon structures is visible. (c) Atomic structure of an ensemble of deposited carbon chains with the number N of carbon atoms. (d) Histogram of the length distribution of deposited carbon chains. (e) TEM images of parts of a two-dimensional crystalline structure formed by parallel carbon chains deposited on the substrate. (f) Period of the structure (value of 0.395 nm is displayed) in the direction perpendicular to the carbon chains (obtained from an analysis of the TEM image profile).

distribution function for the lengths of straight linear sections of carbon chains deposited on the surface (Fig. 9e; image obtained using a transmission electron microscope (TEM)).

We identified the chains containing 8, 10, and 12 carbon atoms by comparing their emission wavelengths with data obtained in the approach of [20]. Assuming a linear dependence of the HOMO–LUMO gap on the number of atoms in the chain and taking into account the proportionality of the concentration of carbon chains of a given length to the width of the corresponding Gaussian peak, the observed photoluminescence band can be represented as a superposition of emission spectra of a certain distribution of linear carbon chains (Fig. 9d). It can be seen that the spectrum is dominated by chains containing from 8 to 24 carbon atoms.

The most common ones are straight linear chains of 10 atoms. It is of importance to note that almost all observed linear regions of deposited carbon chains contain an even number of atoms. This is clearly visible in the TEM image (Fig. 9b) and is confirmed by the Gaussian approximation in Fig. 9a. This rule corresponds to selection by the parity parameter of selective bending of polyyne chains along single electronic bonds (Fig. 9c). Single bonds are 'weaker' than triple bonds, so the stress accumulated in the chain, the ends of which are coupled to metal nanoparticles by triple bonds, manifests itself in kinks in some single bonds. However, the number of carbon atoms between any two one-electron bonds is even.

It is also clearly seen that the lengths of the deposited straight sections of carbon chains significantly exceed the theoretical limit of five to six atoms for individual carbyne fragments. Linear sections of carbon chains containing up to 24 atoms, free from Peierls deformation, can be reliably distinguished [67]. The total lengths of the chains, including curved sections (Fig. 9e), may be as large as several ten nanometers, which is in line with X-ray diffraction data. Parallel linear carbon chains form a regular two-dimensional crystal structure. The profile of such a two-dimensional carbyne crystal is presented in Fig. 9f. The period in the direction perpendicular to the carbon chains/wires turned out to be 0.395 nm with good accuracy. The two-dimensional crystalline phase of carbyne is obtained by simply drying drops of a colloidal solution containing metal-stabilized carbon chains deposited on a fused silica glass substrate. No additional stabilization means were used.

3. Electrophysics in synthesized 1D-carbon configurations. Implementation mechanisms and models: results and discussion

3.1 Basic principles

In general, the stability of any linear system (of length r) is determined in theory on the basis of the introduced Tersoff potential $\Phi(r)$ [9, 23], which characterizes the interaction between atoms (with numbers m and n) at the chain ends through a sequence of intermediate interactions of neighboring atoms.

An analysis for carbon based on this approach shows that, for a linear chain of 3 to 20 carbon atoms (the maximum length is $r \approx 2$ nm), the value of this potential (in volts) for the outermost atoms is in the range $\Phi(r) \sim 3 \times 10^{-16}$–$26 \times 10^{-16}$ V, respectively. This potential generally characterizes the stability of a linear structure in a liquid medium with respect to twisting into a coil due to symmetry factors, surrounding interactions that act on all sides on the atoms in the chain, but which also interact with their neighbors.

However, the force of interaction $F(r)$ between the outermost atoms in the chain has a physical meaning: $F(r) = -\mathrm{d}\Phi(r)/\mathrm{d}r$. Estimates of the stability of the 1D-structure with respect to its length yield the value of the force $F(r) \sim 10^{-4} - 10^{-6}$ N for the above values of the potential $\Phi(r)$. For a colloidal system with carbon atoms (for example, in water/ethanol), this force should be compared with the surface tension forces leading to twisting of the 1D structure, especially under conditions of asymmetry at the boundary with a solid substrate. These latter forces are of the order of magnitude (at a temperature of 300 °C) $F \sim 10^{-6} - 10^{-7}$ N, i.e., the 1D structure is quite stable with respect to such a disorienting effect, especially under the effect of an applied additional external field $\mathbf{E}_0$, which creates a corresponding stabilizing asymmetry in the selected 1D direction.

Thus, according to general thermodynamic concepts, such systems as a whole can have a dominant orientation in 1D structures. This is also facilitated by symmetry factors. For example, in the case of a colloidal system, the same forces act on the carbon chain from all sides, balancing each other, or such induced anisotropy in the orientation of atoms in one direction is due to external forces (for example, an applied electrical field, as in our case) and boundary conditions: a special geometry of roughness on the surface onto which carbon atoms are deposited. The fundamental solution to this problem is to implement interactions with metal atoms connected to carbon atoms at the ends of the carbon chain and acting on them as a stretch. In this case, more complex configurations are possible (the appearance of 2D pieces due to various mechanisms of interaction with the environment), while generally the predominant 1D direction persists as a whole. These situations are modelled below (see Section 3.2).

Since we are focused on 1D structures with sp-hybridization, carbon nanotubes, especially single-walled ones, can also be included in this class [68]. However, they are not considered as well as other structures are: graphene, fullerenes, and their various configurations, although it is the electrophysical properties of these structures that differ in a number of fundamental features with extreme manifestations, including possible superconductivity, ferromagnetism, photoconductivity, etc. [68, 69]. This is determined by the specific configuration of the valence band and conduction band with a corresponding modification of the Fermi level, including their contact at one point, which is typical of semimetals [70]. Therefore, carbon structures can feature very high controllable electrical conductivity [70], including an analogue of semiconductors with donor-acceptor doping.

Chain carbon is one such system, including various options for both the angular orientations of its individual linear fragments of various lengths and the chain structure (macromolecule model) taking into account the corresponding binding energy of carbon atoms [71]. The band gap value was varied with the manifestation of the effects of quantum dimensional electrical conductivity [71, 72].

Study [71] reports calculations for carbyne chains at various chain deformation energies — for carbon atoms in parts of each cell consisting of two atoms. The density of electronic states is determined for various cases, depending on the change in the bond length in the carbyne chain, and an increase in the value leads to an increase in the band gap. The electron density of states (Perdew–Burke–Ernzerhof functional: PBE) and bond length alternation (BLA) in carbyne were calculated in the density functional theory in the local density approximation (LDA) and the hybrid exchange-correlation functional of Heyd–Scuceria–Ernserhof (HSE). The last functional predicts a stronger change in bond length [71].

Electronic energy spectra for carbon nanotubes (CNTs) with a periodic structure/lattice (with a set of parts of two C atoms) in the presence of an external transverse electric field with strength $E = \gamma_0/ea$ (where γ_0 is the transfer integral between the π-orbitals of adjacent atoms carbon, a is the lattice constant, and e is the electron charge) are presented in [73] with a discussion of the presence of Brillouin zones (the first zone) and the dependence of the resulting Bragg gap on the field E.

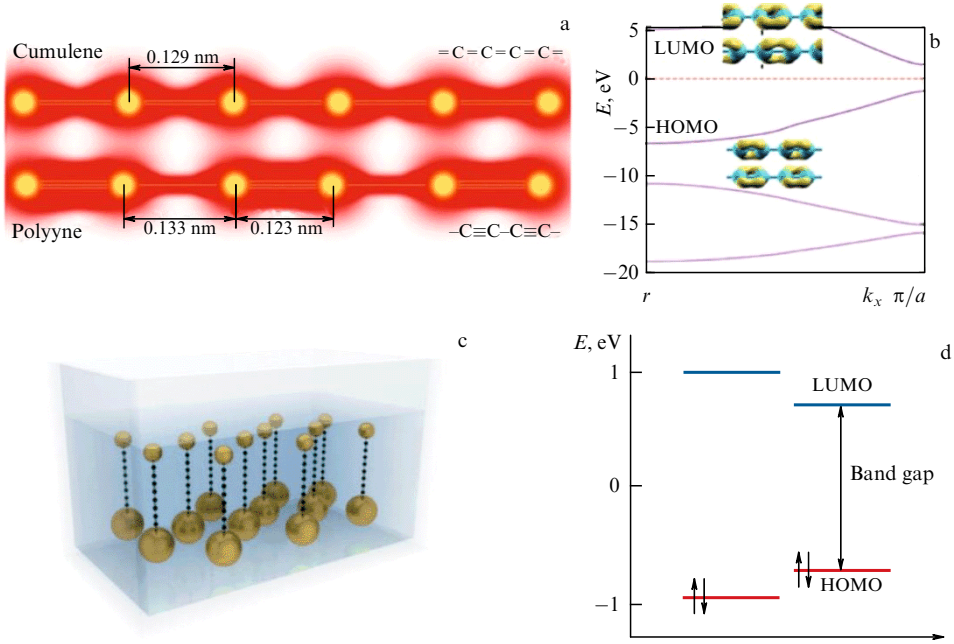

Figure 10. (a) Schematic distribution of electron density in cumulene and polyyne allotropes of monoatomic carbon. (b) Band structure of an infinite polyyne chain (according to our *ab initio* calculations) and doubly degenerate HOMO, LUMO orbitals. (c) Concept of stabilization of monoatomic carbon chains by gold nanoparticles of various sizes in a colloidal solution. Particles are not presented to scale. (d) Energy level structure of a finite polyyne chain consisting of 14 carbon atoms with two gold nanoparticles attached to its ends.

To analyze synthesized carbon structures, methods of Raman/giant Raman scattering and luminescence in such structures are used [74–76], although, in the absence of a band gap, the latter effect does not appear [77].

The issue of stabilization of linear carbyne structures as a new phase state is one of the key problems for the electrophysics of 1D states. Indeed, Landau's theory of phase transitions [23, 78] shows that such structures are unstable and, even with minor fluctuations, twist into coils, unless some external stabilization mechanisms are operative, including symmetry factors and environment.

There are different ways of such stabilization, which was discussed above, including the synthesis of long carbyne carbon chains inside carbon nanotubes (see, for example, [79]). However, we only consider the coupling of carbon atoms with atoms/nanoparticles of noble metals (gold — Au, silver — Ag), which stabilize the carbon chain by stretching the 1D structure with heavy anchor atomic groups at the chain ends. In this approach, a record length of 44 atoms (~ 5 nm) has been attained [80], with distances between neighboring carbon atoms in polyyne of $\sim 0.123-0.133$ nm, with a lattice constant of ~ 0.256 nm.

Calculations [71] show that polyyne with an infinite chain is a direct-gap semiconductor with a band gap of 2.58 eV. Our *ab initio* calculations of the band structure of stabilized infinite polyyne chains predict the existence of a direct electronic band gap of 2.7 eV at the boundary of the Brillouin zone (see Fig. 10 displaying the structure of monoatomic carbon chains).

As noted above, the designations LUMO and HOMO indicate the lowest unfilled level of the conduction band and the highest filled level of the valence band, respectively, for molecular orbitals (see [65, 66]).

It is expected that polyyne chains, being direct-gap semiconductors, will exhibit unusual optical properties with a giant nonlinear optical response [81]. Indeed, unlike graphite or graphene, which are strong absorbers and do not emit light, and carbon nanotubes, where the multivalley band structure leads to dark excitons that suppress luminescence, one-dimensional carbon structures and crystals are promising because of their ability to emit visible light. Photoluminescence spectra of carbon chains at room temperature exhibit a sequence of broad maxima corresponding to chains of various lengths [76]. The band gap of finite-size linear chains depends strongly on the number of carbon atoms in the chain, being larger in shorter chains. In straight polyyne chains containing from 8 to 24 carbon atoms, the band structure is reduced to a sequence of discrete energy levels and is similar to molecular orbitals. The gap between the HOMO and the LUMO varies in the range of 2–4 eV. This leads to a large spectral distribution of allowed optical transitions in such systems.

In our case, stable polyyne chains were synthesized by laser ablation in a colloidal solution. Mechanical stabilization of sp-carbon is achieved through electronic bonding of carbon chains with edge gold nanoparticles. When applied to a substrate, the stabilized chains exhibit straight sections, the length of which significantly exceeds the theoretical limit for a free, stable, monoatomic carbon chain. High-resolution transmission electron microscopy reveals straight linear carbon chains, sometimes longer than 5 nm.

It is also important to note that, if the sizes of metal nanoparticles at opposite ends of the carbon chain are different, the difference between their work functions leads to charging of the carbon–metal nanoparticle complex, which acquires a stationary dipole moment. This dipole polarization provides an additional instrument for ordering the chain using an applied external voltage.

In our experiment [82], carbon chains with gold (Au) atoms/nanoparticles in a colloid, when deposited onto a solid substrate, were preliminarily ordered in a constant electric field, which made it possible to obtain long parallel polyyne chains on the substrate (Fig. 11).

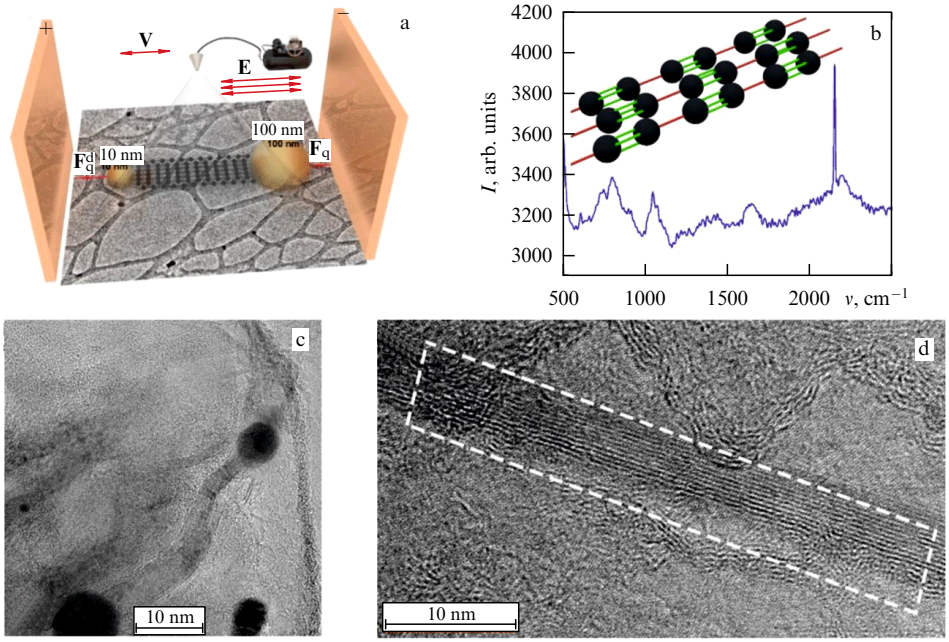

Figure 11. Alignment of linear monoatomic carbon chains under the effect of an external electric field. (a) Experimental setup. (b) Raman spectrum of the resulting structure. (c) TEM image of this structure on a solid surface. (d) A clearly seen part of a 2D ensemble of 1D-carbon structures.

Such controlled deposition of 1D structures on a solid surface and their stabilization are quite feasible in the scheme presented in Fig. 11, which also displays an image of the obtained structure in an electron microscope and its Raman spectrum corresponding to the depicted linear monoatomic carbon chains [82].

Thus, as follows from everything presented above, fixed and isolated 1D carbon structures are actually realized in experiments. They are by no means reduced to separate sections mixed with other blocks in a chaotic configuration.

It should be noted that the length of the bundle of carbon chains in its central part exceeds 40 nm. Based on this observation, we can assert that such an ensemble forms a kind of one-dimensional van der Waals crystal. There is a great deal of interesting physics here, including electrical parameters, which is, however, beyond the scope of this review.

We only note that charged excitonic complexes (trions) [24] will probably be formed in our system due to the proximity to metal nanoparticles, which can supply carbon chains with additional charge carriers. A variational calculation (cf. [24]) predicts the splitting of an exciton into a positively charged trion with a binding energy of about 15 meV and the splitting of a positive-negative trion with a binding energy of 25 meV, values which agree well with experimental data. The strong dipole polarization of approximately half of the carbon chains stabilized by gold with different sizes of its nanoparticles at the carbon chain ends is confirmed by their alignment in an external electric field.

Thus, the presence of additional charges localized at the ends of some chains is beyond doubt. It is expected that the spectral-integrated intensities of negatively charged (X−) and positively charged (X+) trion transitions will be lower than the integral intensity of the neutral exciton transition [36].

Indeed, statistically, at equal concentrations of gold nanoparticles with sizes of 10 and 100 nm, it may be expected that only half of the carbon chains will be attached to them with different radii and, therefore, will be strongly polarized. In such polarized chains, the two lowest-energy optical transitions will be either positively or negatively charged trions. Since each chain is divided by kinks into several straight parts, neutral excitons nevertheless can form in the central parts of the polarized chains. It may be assumed that the sum of the integral intensities of the X− and X+ lines should be less than or equal to the integral intensity of the X line.

This demonstrates the high potential of synthesized polyyne chains for optoelectronic applications, especially in nanolaser and single-photon emitters. In addition, the observation of radiation-active excitons in extremely long one-dimensional carbon crystals is of great fundamental interest. However, detailed studies are needed in this area to fully reveal the properties of excitons and trions in carbon chains.

It is most interesting to note that, at the liquid helium temperature, a well-pronounced fine structure appears at the peaks of broad resonances corresponding to polyyne chains of various lengths in the photoluminescence spectra of deposited carbon chains (see Fig. 7). This fine structure invariably consists of a high-amplitude narrow peak accompanied by two low-energy satellites, which can be attributed to excitonic resonance and two trion resonances, respectively. Time-resolved photoluminescence spectra show that the radiative lifetime of the observed transitions is on the order of 1 ns, similar to the data reported for excitons in carbon nanotubes [83].

For low temperatures (~ 4 K), carbon 1D structures configured as thin linear monoatomic chains were observed in [36] with a triplet spectrum repeating for various wavelengths of exciting optical radiation, similar to the case illustrated in Fig. 7. This observation enables a conclusion that, in the absence of temperature fluctuations, such triplets are completely stable objects but depend on the wavelengths of the incident light.

These ideas shape the prospects for the practical use of carbon 1D structures acting as molecular wires for micro- and

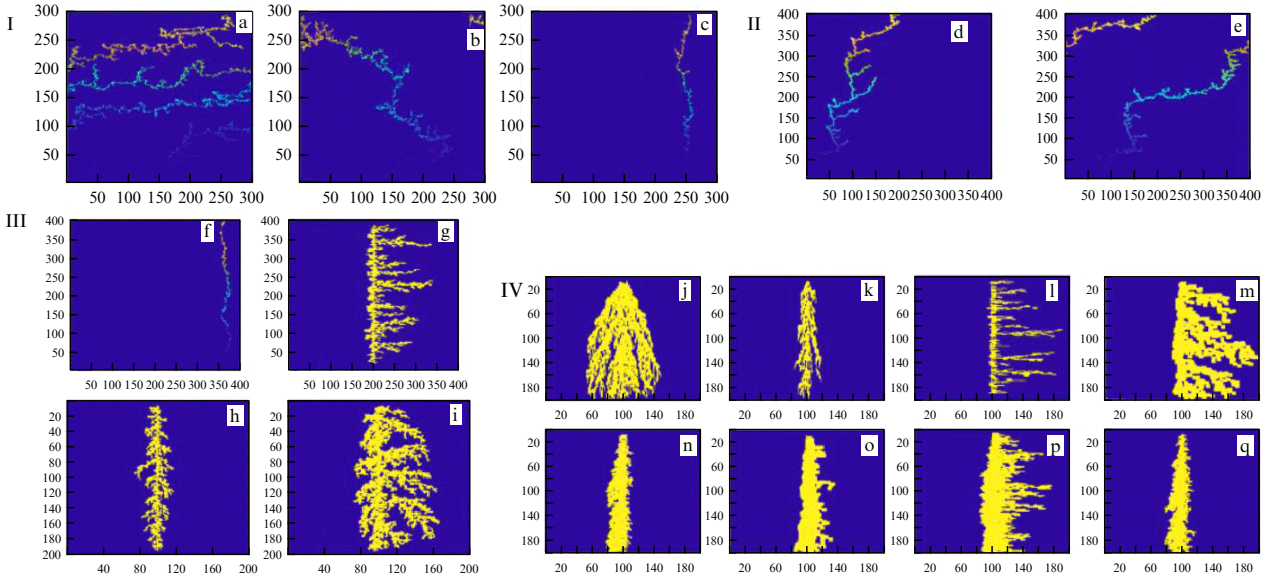

Figure 12. Results of calculations of fractal structures using the DLA model with preferred growth highlighted. I. Filaments of length 2 (parts of two atoms): (a) horizontal growth; (b) diagonal growth; (c) vertical growth (up). II. Diagonal filaments of length 3 (parts of three atoms): (d) upward growth; (e) sideways growth. III. Vertical filaments of length 4 (parts of four atoms): (f) upward growth; (g) growth to the right side; (h, i) symmetric growth to the right and left sides but with different rates. IV. Filaments of length 5 (parts of five atoms): vertical growth from the original source at the top (see Fig. j) but at different rates and in different directions: (j–q).

nanoelectronics, polaritonics, spintronics, and photonics, taking into account the effects manifested in the combination of the functional characteristics of 'electrophysics + optics' with their specified variation for various elements and devices, including printed-circuit electronics [84–88].

3.2 Modeling of fractal structures with 1D-dominant orientation, including orientation set by an external field

In this area, great opportunities for studying such complex structures are provided by analyses based on corresponding computer models. We used two models to explore the emerging fractal structures (cf. [89–92]): first, the diffusion model and, second, a model with diffusion-limited aggregation (DLA). It was assumed that the linear carbon structures (central filaments) have the form of chains of 8 to 24 atoms joined in these chains into successive molecular pieces consisting of two and four atoms, to which, in accordance with the model, fractal nanothreads were 'adjusted.'

The results of such modeling are shown in Fig. 12 (DLA model approximation). Molecular carbon structures were considered that consisted of various numbers of atoms (the length of the filament in the pieces) and were located at various sites on the substrate relative to the axis of the linear structure under conditions of different growth rates and growth directions — in practice, relative to the applied external field that determines the dominant direction of growth (all qualitative geometric parameters are indicated in the captions to the figures).

Model images of the resulting structures shown in Fig. 12 generally correspond, for example, to the structures from the experiment and its interpretation displayed in Fig. 7 and 8.

3.3 Electrophysical characteristics in modeling a 1D structure: quantum approach

Quantum mechanical tunneling of electrons in an inhomogeneous structure can occur both inside a nanocluster and from a nanocluster to neighboring nanoclusters. Resonance tunneling refers to tunneling in which the transmission rate of electrons through a structure abruptly reaches a maximum at certain energies. For electrons with an energy approximately corresponding to the virtual resonance energy level of a quantum well, the transmission coefficient is close to unity. It is for this reason that an electron with such a resonant energy can pass through a potential barrier without being reflected. This resonant phenomenon is similar to that occurring when light passes through a Fabry–Perot optical resonator and/or in transmission line resonators with microwave capacitive coupling, i.e., similar to Klein passage without reflection (see, for example, [23, 24, 94–96]).

We now consider 1D structures and their electrical and functional characteristics of various types for the case of a simple Kronig–Penney model [23] (cf. [24, 65, 66, 93]). The main results obtained are presented in Fig. 13 (see [28, 29]) for the transmission of charged particles in the model of spherical nanoclusters.

The calculation was carried out in the standard quantum approach [23, 24], so we omit the corresponding equations and only present the values of the key parameters of the problem.

The transmission of the electron flux T in a quasi-1D structure consisting of nanoclusters as a function of the electron energy E (based on the normalized ratio E/E_F, where E_F is the Fermi energy) for a regular (Fig. 13a) and disordered (Fig. 13b) structure is determined by numerical values of the following control parameters of the problem: Wigner–Seitz parameter $r_s = 2.1$ ($r_s \sim 1/N_e^{1/3}$, where N_e is the density of valence-electron states ($N_e = 40$)), $m_{eff} = 1.4$, $m_e = 0.708$ MeV, $E_F \approx 6$ eV, $\hbar/\tau = 10^{-3}E_F$, and distance between two clusters $\ell \approx 20$ nm.

As can be seen, the electronic transmission spectrum of such a superlattice consists of a number of spectral bands (for example, Fano resonance/interference). For the calculation, we used the transfer matrix approach with the Morse potential $V(r) = D_e[1 - \exp(-a(r - r_0))]^2$, where D_e is the

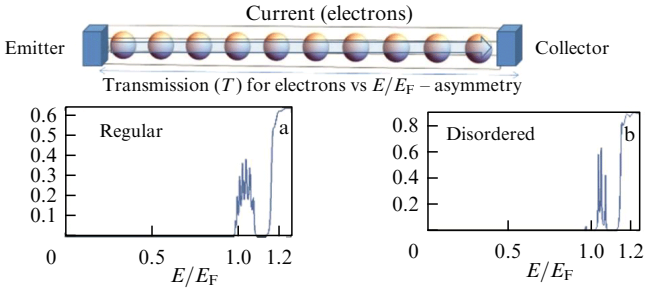

Figure 13. Electric conductivity in the quasi-one-dimensional case. Electrical quantum tunneling through 10 nanoclusters (Kronig–Penney 1D model along the longitudinal z-axis), i.e., an array of nanoclusters (nanocluster superlattice) between two microcontacts (emitter–collector) in both ordered (a) and disordered (b) cases.

potential well depth, $a = \omega_0\sqrt{m_e/2D_e}$ is the potential well width, ω_0 is the frequency of the harmonic oscillator, and r_0 is the position of the local minimum (for the equilibrium state).

The results of calculating the current-voltage dependence are presented in Fig. 14.

As soon as the voltage at the microcontacts of the quantum-well structure (see top diagram in Fig. 13) goes beyond the boundaries of the corresponding energy of one of its resonant states, the tunneling current increases (region *1* in Fig. 14).

With a positive displacement along the z-axis of the right microcontact relative to the left microcontact, the electron state energy passes through a resonant energy level in the system. When the Fermi energy E_F passes through this resonant energy, large currents are generated due to the enhanced transfer of energy from left to right between the microcontacts. This leads to a significant increase in current (region *2* in Fig. 14). If the displacement of the microcontact increases even further, the current between the microcontacts stops flowing when the E_F level drops below the edge of the conduction band. As a result, current noticeably decreases with increasing voltage, which leads to the appearance of a region of negative differential resistance or to significant suppression of the current (region *3* in Fig. 14). With further displacement of the microcontacts, the current increases again, since the particles acquire kinetic energy sufficient to overcome the potential barrier, and breakdown may occur (region *4* in Fig. 14).

Electric current I between microcontacts is defined by the formula

$$I = eS\int_0^{p_F}\frac{\hbar k_z}{m^*}\,T(k_z)\,\frac{2\pi(p_F^2-\hbar^2k_z^2)}{(2\pi\hbar)^3}\,\hbar\,\mathrm{d}k_z\,,$$

where S is the cross-sectional area of the structure, p_F is the Fermi momentum, and $T(k_z)$ is the transfer matrix for the coefficient of electron flow transfer along the direction of the wave vector k_z.

Thus, in the 1D structure, the electrophysical dependences can be controlled, which is of importance for various practical applications in nanoelectronics.

A special case of the 1D structure for our problem is the long linear carbon chains (LLCCs) already discussed above, which represent a new allotropic phase of carbon, carbyne. We discuss it with more detailed information about the measured Raman spectra in subsequent Section 4.

We also note that the very shape of nanoparticles/nanoclusters and its deformation determine the distribution

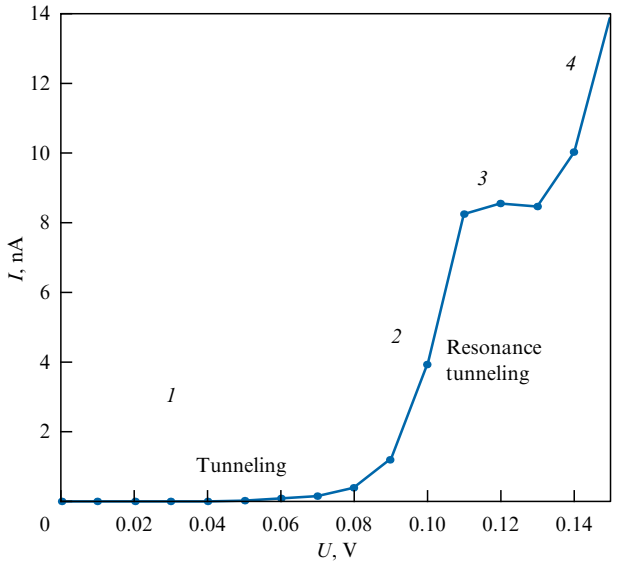

Figure 14. Current-voltage characteristic of a quasi-1D structure consisting of nanoclusters (see explanation in the text).

and relative arrangement of energy electronic states and their density in thin-film 2D systems [23, 24, 29–31, 65, 66]. In the core-shell structure model, in such cluster systems of various elemental compositions, this leads to strong dimensional effects and bound states for charge carriers near the Fermi level (cf. [94]). Such bound states of electrons are of interest in regard to the feasibility of achieving a superconducting state. However, we skip this feature, given our emphasis on considering processes in carbon 1D structures.

3.4 Experimental demonstration of current-voltage dependences of 1D structures

The electrical properties of linear-chain carbon (carbyne) were studied in Yu S Prazdnikov's PhD thesis (2005, Moscow State University), see also [97–99], with a focus on measurements along and across chains. Injection and field characteristics with contact barriers located at the carbyne-dielectric interface were explored and the production of a crystal formed by charge-topological solitons, macroscopic-size quasiparticles, in the absence of random interweaving of carbon chains was discussed. In a flat contact of a carbyne film with SiO_2 with a thickness of 0.1 μm, a volumetric current density of up to 0.4 A cm^{-2} was obtained at an applied field strength of 10^5 V cm^{-1}. The calculated work function of electrons from carbyne in the thermionic emission model was 0.4–1.6 eV. Interestingly, a stepwise dependence of the resistance of a carbyne film on its thickness and an anomalous injection/emission ability of such carbyne films were detected. The results of the experiments allowed the authors to assert that they had discovered a new universal mechanism for reducing contact barriers at the border with carbyne based on a field 'built in' to the carbyne, independent of the band parameters of the material. A band model of this mechanism shown in Fig. 15 was proposed [98].

In [100], in films of linear-chain carbon 100 nm thick, the structure and electrical conductivity of curved carbon chains on various metal substrates were analyzed. These chains were obtained by pulsed plasma deposition. For these structures, the differential current-voltage characteristic $\mathrm{d}I/\mathrm{d}U$ was measured in the experiment and the effects of oscillations

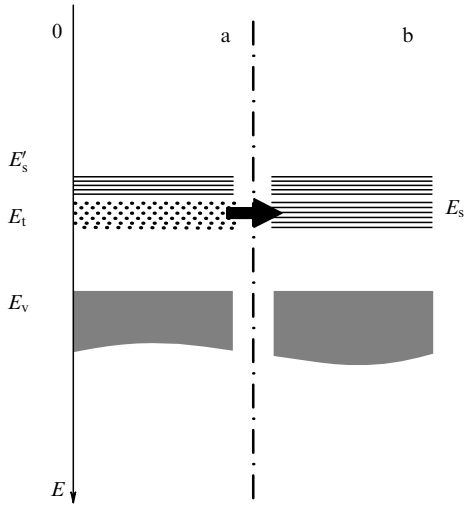

Figure 15. Band model of an oriented carbyne film for electrical conductivity in the direction transverse to the carbon chain. (a) Spontaneously generated solitons are the states localized in the chain, forming trap band E_t inside the carbyne band gap. (b) At some thickness of the carbyne film, a soliton lattice is formed, and states of the soliton are delocalized with the formation of a new band E_s in the direction transverse to the chain, which is wider than soliton band E'_s located below.

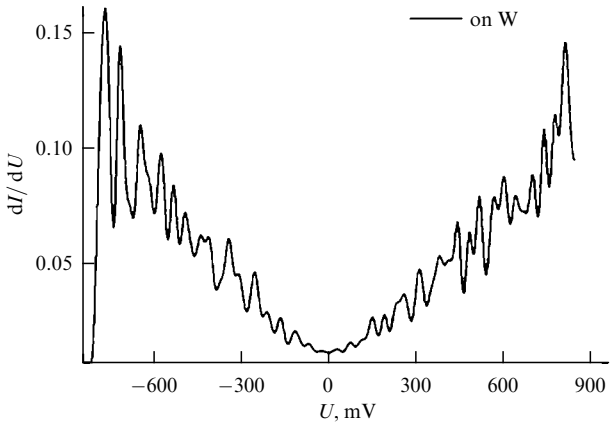

Figure 16. Typical plot of tunneling oscillations of electrical conductivity for a film of linear chain carbon deposited on a tungsten substrate.

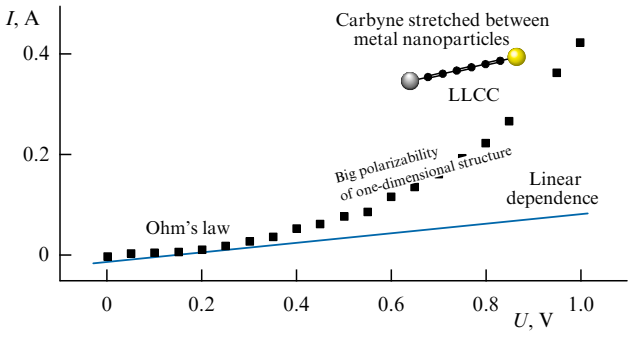

Figure 17. Current-voltage characteristics of thin films of the linear Au/Ag-Carbon structure (i.e., carbyne structure between Au and Ag atoms at its ends) 30 nm thick on a glass substrate.

with approximately the same periods were observed, depending on the value of U in the range from −900 to +900 mV at room temperature. Figure 16 displays a typical differential current-voltage characteristic of films obtained in [100]. The experimental conditions corresponded to the case when the applied voltage was comparable to the work function of electrons from the substrate surface.

The experimental results were considered using a model based on the formation of one-dimensional charge density waves along the carbon chain. Electrophysical characteristics were calculated for a number of configurations: a single cumulene consisting of four carbon atoms, a double cumulene of 10 carbon atoms, a single polyyne (four carbon atoms), and a double polyyne (10 carbon atoms). A double chain means in this case that a bend occurs between the linear chains with corresponding bending angles, which affect the electrical characteristics of such structures.

We also present here one of our demonstrations of experimental results for current-voltage characteristics, namely for the Au/Ag complex with carbon, which leads to the synthesis of a long linear carbon chain, an LLCC (see [4, 5, 10, 28]), shown in the upper part of Fig. 17.

The increase in electrical conductivity seen in Fig. 17 at $U > 0.2$ V compared to the recorded linear dependence in accordance with Ohm's law at small U can be explained by the high polarizability of the linear-dimensional 1D structure (LLCC) in an increasing external field, which arises in this case. We actually observed suchlike dependences for similar 1D structures formed from other materials, in particular, for bimetallic nanostructures [4, 5, 10, 26, 101] with a change in the mechanism of electrical conductivity (from tunnel to thermally activated jumps), depending on the distances between nanoobjects in their linear arrangement. However, in our case, the 1D structure was stable, and phase transitions in it at such voltages U were hardly possible due to the structures discussed in Section 3.2 (cf. [23]). On the contrary, it is the additional 1D structuring that could be implemented with the application of an external field. Such ensembles of 1D structures demonstrate a tendency towards superconductivity; in particular, it was observed in cuprates [102].

In our other experiments conducted with monoatomic cluster structures of various compositions (see, for example, [26]), the linear dependence $I(U)$ persisted throughout the entire range of measurements for various configurations of nano-objects. However, in thin-film cluster systems with metals and semiconductors, the electrical conductivity increased greatly (up to a factor of 10^4), depending on the surface topology of the nanostructures synthesized in a laser experiment.

Of particular interest here are the measurements of photoinduced electrical conductivity in LLCC structures excited by additional irradiation of a carbon sample with weak optical radiation (power not exceeding fractions of a μW) in comparison with nanocluster structures of other substances (for example, gold (Au)). The results are shown in Fig. 18. A strong increase in the efficiency of the current-voltage characteristics is seen for LLCC samples compared to a nanocluster thin-film gold system. In the case of an LLCC, the initial current-voltage characteristic was virtually zero. The resistance of the LLCC samples dropped from 700 to 6.5 MΩ, i.e., more than a factor of 100, while the resistance of gold structures decreased from 390 to only 80 MΩ. This data also confirm that the LLCCs obtained in the laser experiment are quite real stable objects with unique characteristics suitable for use in applied problems.

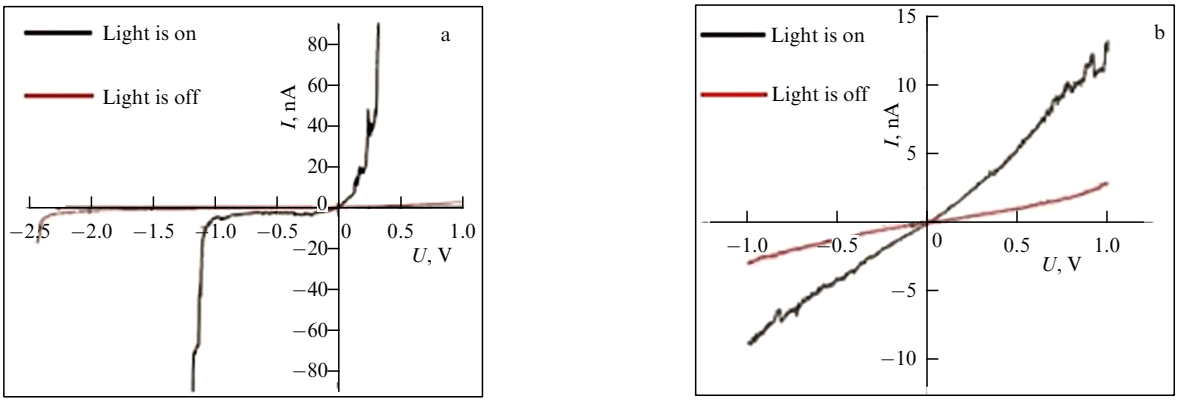

Figure 18. Current-voltage dependences for photoinduced conductivity (in the field of low-power optical radiation in the green region of the spectrum — light is on): (a) for LLCC samples and (b) for a nanocluster structure of gold atoms.

4. Changes in the spectral characteristics of 1D carbon structures under the effect of laser radiation

We now consider in more detail the features of various realized configurations of carbon 1D structures measured using optical spectra. It is these configurations that determine their functional characteristics expressed in terms of optical and electrical parameters.

We analyzed the structural features of the sample surface in the laser irradiation region employing Raman scattering spectra obtained using the Ntegra Spectra probe nanolaboratory (excitation wavelength of 473 nm, power of 50 mW, measurement duration of 100 s).

For glassy carbon, the data depended on only the specifically selected measurement area on the sample surface which was exposed to laser radiation.

Spectral bands in the range of 1350–1580 cm^{-1} are typical for shungite targets (Fig. 19). The change in the ratios of the magnitudes of the peaks in the spectrum as the laser exposure energy increases indicates a change in the structure of the material, depending on the exposure conditions. The deviation of the spectrum band center from 1600 cm^{-1} is apparently associated with a decrease in the size of graphene layer stacks (cf. [6, 16, 19–21, 103]).

The initial sample featured a low-intensity G-peak characteristic of graphite, which is located in the region of 1582 cm^{-1} (see Fig. 19). The resulting nano- and microstructures are associated with carbon with sp^2 hybridization: the narrowing of the peaks and their shift to shorter wavelengths indicate a restructuring of carbon-carbon bonds in the so-called 'breathing' modes [9, 11, 37, 61]. As the energy density of the laser radiation irradiating the sample increases, a decrease in the intensity of the D-peak (1380-cm^{-1} region), characteristic of the amorphous state of carbon, is observed, and peaks also appear in the region of 600–1000 cm^{-1} due to the modification of the structure of the material and the appearance of mechanical stresses in it (cf. [9, 39, 104]).

Changing the speed of laser beam scanning over the sample surface led to varying the ratio of peak intensities without a significant rearrangement of the Raman spectra themselves. This is apparently due to structural phase transitions in the system at various energy parameters of laser exposure.

In the experimental setup with laser ablation in a liquid that we use, replacing the liquid phase of the colloid can significantly alter the process of particle fragmentation and the conditions for carbyne formation.

However, the use of distilled water for these purposes has a number of significant advantages, since it makes it possible

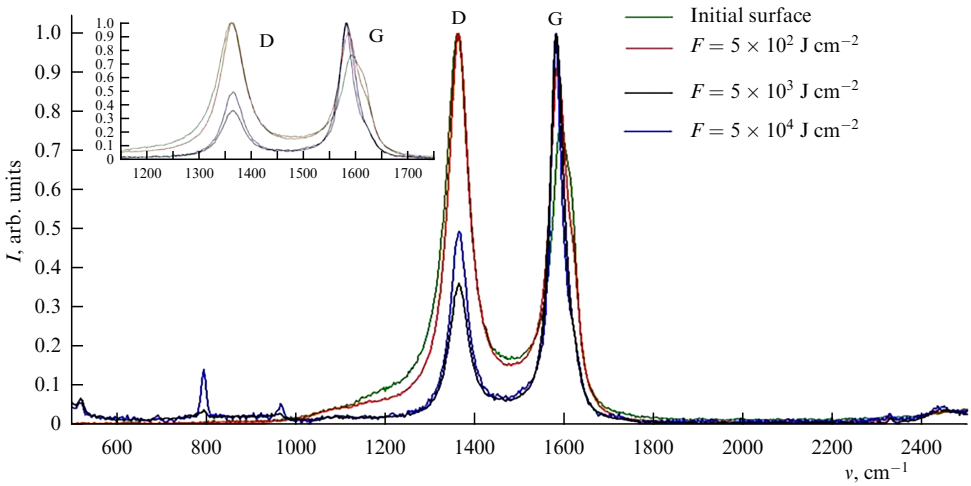

Figure 19. Normalized Raman scattering spectra for the original shungite sample and for areas affected by laser irradiation with various energy densities F, J cm^{-2} (shown at the top right). In the inset displayed in the upper-left corner, central peaks of standard spectra for the shungite sample are highlighted.

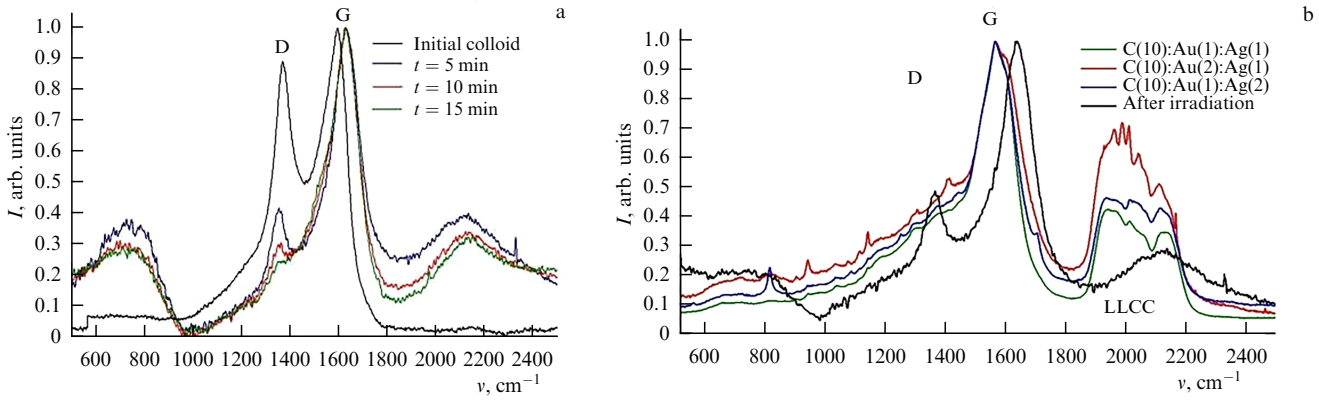

Figure 20. (a) Raman scattering spectrum (RSS) of the initial colloidal system with an LLCC and subsequent systems obtained after irradiation with nanosecond laser radiation (λ = 1.06 m) with an intensity of 10^6 W cm^{-2} and exposure time t ranging from 5 to 15 min (indicated at top right). (b) RSS after exposure for t = 5 min to pulsed millisecond laser radiation (λ = 1.06 μm) with an energy of 1 mJ but with a different quantitative composition of proportions of C, Au, and Ag atoms (shown at top right), which determines the effectiveness of LLCC implementation.

to avoid the formation of new carbon phases due to the reaction of carbon atoms and molecules with molecules of the environment. Even if compounds with oxygen or hydrogen are formed during laser exposure, they are volatile compounds that escape from the laser exposure area and, in general, the volume of liquid, without affecting the 1D configuration.

In the original colloidal system that we studied (Fig. 20), two peaks are clearly visible: D (1380 cm^{-1}) and G (1580 cm^{-1}), corresponding to the original shungite sample. The LLCC structure corresponds to a spectral region in the range of approximately 1900–2300 cm^{-1}, depending on irradiation conditions and LLCC composition.

As the laser exposure time increases (Fig. 20a), the intensity of the D peak begins to decrease significantly; with an exposure time of 15 min, the shape of the spectrum in this region completely transforms into the modified (D+G) band typical of carbyne [9, 11, 44]. Concurrently with the transformation of the peak, a shift of the G peak to 1610 cm^{-1} is observed; the D peak is shifted to the region of 1360 cm^{-1}, which may be indicative of the breaking of bonds between the emerging graphene layers [38, 39]. The appearance of an intense band in the range of 600–900 cm^{-1} is apparently associated with the deformation of carbyne chains, the structure of which is most clearly visible in the spectral range of 1900–2300 cm^{-1} [4, 5, 9, 11, 44].

On the other hand, the efficiency of LLCC formation significantly depends on the interactions of atoms with Au and Ag atoms fixing the LLCC in various proportions (Fig. 20b).

The polyyne structure of atomic carbon chains is reflected by bands of stretching vibrations of triple bonds (−C ≡ C−) in the range of 2100–2300 cm^{-1} and bending vibrations at 800 cm^{-1} [6, 9, 16, 104]. Thus, the shift of this peak (2100–2300 cm^{-1}) to the short-wavelength region during laser irradiation of the colloidal system is explained by a change in the length of the carbon chain.

The cumulene structure (= C = C =) is manifested in absorption peaks at 1950 cm^{-1}. The absorption band in the region of 1600 cm^{-1} can be associated with the fundamental absorption band for the cumulene form of carbyne (regular zigzags consisting of linear parts of four carbon atoms). These structures can also be rearranged under laser irradiation.

It is necessary to take into account that (in accordance with [9, 19, 37, 59–61, 104]) the formation of linear carbon chains can lead to the formation of structures with sp^3 hybridization. In our case, when a colloidal system is exposed to laser radiation, agglomerates can appear that consist of carbyne chains linking carbon nanoparticles into clusters and complexes, which is reflected in the spectra in the region of 600–900 cm^{-1} and 1900–2200 cm^{-1}. It is of importance to note that, when laser radiation with a nanosecond pulse duration directly affected the surface of a shungite target, no traces of carbyne formation were detected.

After deposition from a colloidal system onto the surface of a solid substrate, the spectrum shape changes significantly. Although central peaks of the initial colloid are not shifted after its irradiation, a fairly intense G-peak located in the region of 1580–1610 cm^{-1} is observed in the Raman spectra of the colloidal system before and after laser irradiation. The D peak (1380 cm^{-1}) is observed for all samples, although its intensity varies, depending on the laser exposure conditions. The peaks corresponding to carbyne with a polyyne bond narrow into the range of 2100–2200 cm^{-1} (see [4, 5, 11, 44]).

This behavior of the spectrum suggests a conclusion that, in the process of evaporation of the colloid on the substrate, the carbyne chains transform into carbon structures with sp^2 hybridization (cf. [59–61]).

With increasing exposure time, bands in the range of 800–900 cm^{-1} corresponding to bending vibrations appear in the spectra [4, 5, 9].

Consequently, it can be argued that, in the process of drying a colloid drop on a solid surface, linear carbon chains can be transformed into complex molecules: ‘coils’ and ‘globules’ (cf. [38, 45–48, 59–61]).

Thus, the characteristic peaks of these spectra for LLCCs are clearly visible, not only in the colloidal system itself but also when deposited on a solid surface. On the other hand, the very conditions of laser irradiation of LLCCs of various compositions modify the observed spectra which determine the specific state of the LLCC.

5. Conclusion

One-dimensional carbon structures, being low-dimensional/linear dipole systems with high polarizability, are candidates

for achieving high electrical conductivity in thin films on a solid surface, including trends toward the transition to high-temperature superconductivity in various hybrid systems with various/corresponding chemical/elemental compositions (see, for example, [23, 24, 105]). However, the problem is that the instability of a one-dimensional system due to steric factors, helicity, and folding into globules with the corresponding density distribution of objects, etc. leads to polydispersity of a macromolecular system with a spherical and/or branched structure, which eliminates these advantages.

Although it can be assumed that the allotropic phase of carbon, carbyne, may appear simply as weakly controlled pieces of various lengths with polyyne or cumulene carbon bonds combined with other types of hybridization, in our case, this is apparently not the case. First, we directly observed the dynamics of graphite melting in a laser experiment at temperatures < 4000 °C (see Section 2.3 and Fig. 1). Second, the entire set of the obtained Raman spectra and their interpretation (Sections 2.3, 3.1, and 4) suggest that, indeed, 1D-carbon structures were actually synthesized in our experiments and were stable with the realized bonding of carbon atoms with noble metal atoms located at the chain structure ends in various controlled ratios according to the percentage of these elements (see, for example, Figs 6–9, 11, and 18–20).

We analyzed above the possible role of some adverse processes associated with diffusion phenomena and showed, on the basis of simulation, that the dominance of the 1D structure in carbon systems can generally be maintained under certain conditions even with the development of diffusion processes and the appearance of fractal structures (models presented in Section 3.2). Taking into account that phase transitions cannot occur in strictly one-dimensional systems [23, 78], the presence of diffusion, leading to the emergence of differently located fractal pieces (nanothreads) of an overall 1D-oriented filamentary carbon structure, allows the appearance of new phase states characteristic of 2D and 3D structures (cf. [23, 24, 48–51, 106, 107]).

Indeed, the manifestation, for example, of nonergodicity in electrical conductivity even in a granular nanostructure significantly enhances the role of certain quantum states (cf. [79, 94, 107, 108]). In particular, new phase states were obtained in forming a long linear carbon chain, notably, cyclocarbon with 18 polyamide atoms (alternating triple and single bonds: $-C \equiv C-$) [39].

Furthermore, new superconductors of various types based on carbon compounds are currently the subject of intense discussion. An example is twisted bilayer graphene when nematicity is violated in a system [19, 37], which is relatively easily achievable in a system containing initially synthesized carbon 1D structures. In a doubly connected body, a ring, the total electric current flowing through it determines the distribution of surface currents in the body. This is also true of systems of any connectivity [94, 108–110].

Depending on the topology, in particular, the boundary shape of nanoclusters, the structure of their electronic bands changes dramatically. This leads to various modes of electrical conductivity, including the tendency towards superconductivity based on new physical principles (cf. metallized carbyne with alternating carbon dimers with copper atoms [47]).

In addition, the Josephson quantum junction [111], which features unique characteristics for superconducting circuits, appears to be very promising specifically with one-dimensional carbon structures in complex compounds (cf. also [112–114]).

In this case, the quantum mobility of electrons along trajectories in spatially inhomogeneous structures/nanocluster systems is represented as the movement of electrons in accordance with the path integral [115].

In classical theory, this is the standard Brownian motion of particles along $x = x(t)$ trajectories in accordance with the Einstein–Smoluchowski equation [23, 94].

In quantum theory, the transition amplitude and probability are determined by the path integral with the corresponding kernel [24, 115]; however, it is necessary to calculate the integral over all trajectories/spatial variables, in contrast to considering each fixed trajectory in classical theory.

However, interference quantum effects with corrective additives, which lead to electrical conductivity for 1D structures, are also of importance [24, 106].

Indeed, on the one hand, in the model of noninteracting electrons with momentum p_0, which, however, are scattered on impurities, for the electron trajectory along a de Broglie tube thickness $\lambda_{dB} \sim h/p_0$, diffusion with coefficient D occurs under conditions of inelastic electron–phonon (e–ph) scattering. At high temperature T, electron–electron interactions (e–e) occur due to their repulsion during the time $t_j \sim \hbar\mu/k_B^2 T^2$, which alters the energy spectrum. On the other hand, at a low energy level $T < (\hbar\omega_D)^2/\mu$, where μ is the chemical potential (Fermi energy), k_B is the Boltzmann constant, and ω_D is the Debye frequency, an additional interference term arises, and the electrical resistance decreases with increasing temperature T. This effect is dominant for a one-dimensional 1D system (similar to the Kondo effect) [94–96].

Phenomena of photoinduced electrical conductivity may occur (cf. [65, 66, 116]) when, under irradiation of such a thin film containing an LLCC and metal nanoparticles with continuous low-power laser radiation (power not exceeding 1 μW), a sharp jump appears in the current-voltage dependence [117] — by a factor of hundreds (currents of tens of nanoamperes at a voltage of a fraction of a volt) — accompanied by a decrease in electrical resistance by hundreds of times due to photoactivation of electronic states in such hybrid clusters, taking into account plasma resonance in metal nanoparticles.

Thus, various modes of electrical conductivity are possible in such 1D systems with linear trajectories of electron motion. These modes were experimentally demonstrated in the references cited above for various thin-film structures deposited on a solid surface.

These observations lend hope that, in external electric and magnetic fields, 1D carbon filament-like systems and their modifications, which we considered (cf. [114]), containing pieces in the form of fractal nanowires that spontaneously break symmetry due to the influence of diffusion, can be of significant importance for various topologically modified structures with superconducting characteristics in carbon-containing compositions. This should determine the corresponding trends in the increase in electrical conductivity in such structures and enable predicting the manifestation of fundamental features in electrophysical properties based on new physical principles for the development of now widely discussed real prototypes of hybrid topological objects with possible superconducting states. Publications reporting research in these areas copiously appear with proposals for various structures and trigger active discussions, including the withdrawal of articles already published in a number of reputable journals (see, for example,

comments in [118]). Arguably, it is carbon-containing 1D complexes in combination with various metals such as high-entropy materials [119] that can be very promising candidates in this area, where fundamental achievements can be expected.

Technologies using laser ablation discussed above are universal, do not require employing expensive vacuum technology, for example, in epitaxial electronics, and are promising candidates for printed-circuit electronics with controllable functional characteristics of synthesized objects, including electrophysical properties. It is the configuration of samples of various dimensionality with a similar surface topology and controllable elemental composition controlled in a laser experiment that makes it possible to set trends towards achieving superconducting states in micro- and nanosized systems; the latter can possibly be used in various next-generation devices and systems, including micro–nanoelectronics and nanofemtophotonics (cf. [14, 25, 55, 114, 116, 120, 121]), notably for the purposes of printed-circuit electronics in general.

The physical principles underlying the development of such systems with fractal electrical conductivity in thin films deposited on a solid surface are discussed in our recent publication [101] (see also [4, 25, 123]). The physical features of inhomogeneous structures with fractal objects have been repeatedly presented in *Physics Uspekhi* (see, for example, [124, 125]). The results of these studies can be of use for various complex carbon structures, especially those containing 1D configurations with various topologies. This offers practical prospects in the development of various solid-state elements for micro- and nanoelectronics and photonics with controlled functional characteristics.

In this regard, processes with superconducting nonlinear charge transport in carbon-containing complexes are very promising. In a recent study [126], for example, photoexcitation was investigated in a thin film of high-temperature K_3C_{60} with ultrafast switching on of the current-voltage response. Such a granular system with nonequilibrium superconductivity between superconducting clusters operates on the basis of a laser–induced superconducting state, which offers new approaches to the development of an optoelectronic platform for ultrafast light-controlled devices. Such control of electron transport in optical circuits is currently of great interest (cf. [127]), and fundamental advances should be expected in this area in the very near future.

It is likely that, based on these science-intensive principles, Russia can gain technological sovereignty in terms of the development of elements and systems of micro- and nanoelectronics and femtophotonics.

The work was prepared with the support of the Ministry of Education and Science of the Russian Federation (topic FZUN-2023-0003) and a grant assigned for the 2019–2020 project allocated to the Federal Center for Research and Development of the Ministry of Education and Science in accordance with agreement no. 075-15-2019-1838 between Vladimir State University and the Ministry of Education and Science. It was also partially supported by the Russian Science Foundation (grant no. 23-12-20004) (https://rscf.ru/project/23-12-20004/). Experimental studies were carried out using the equipment of an interregional multidisciplinary and interdisciplinary center for the collective use of advanced and competitive technologies in the areas of development and application in industry/mechanical engineering of Russian achievements in nanotechnology (agreement no. 075-15-2021-692 of August 5, 2021).

References

1. Yang G (Ed.) *Laser Ablation in Liquids. Principles and Applications in the Preparation of Nanomaterials* (New York: Jenny Stanford Publ., 2012) https://doi.org/10.1201/b11623
2. Abramov D V et al. *JETP Lett.* **84** 258 (2006); *Pis'ma Zh. Eksp. Teor. Fiz.* **84** 315 (2006)
3. Arakelian S M et al. *Bull. Russ. Acad. Sci. Phys.* **81** 1468 (2017); *Izv. Ross. Akad. Nauk Fiz.* **81** 1664 (2017)
4. Kucherik A O et al. *Quantum Electron.* **46** 627 (2016); *Kvantovaya Elektron.* **46** 627 (2016)
5. Kutrovskaya S V et al. *Laser Phys.* **29** 085901 (2019)
6. Cannella C B, Goldman N *J. Phys. Chem. C* **119** 21605 (2015)
7. Arakelian S et al. *Opt. Quantum Electron.* **48** 342 (2016) https://doi.org/10.1007/s11082-016-0608-9
8. Kucherik A O et al. *J. Phys. Conf. Ser.* **1164** 012006 (2019)
9. Amsler M et al. *Eur. Phys. J. B* **86** 383 (2013)
10. Khorkov K et al., in *New Trends in Nonlinear Dynamics. Proc. of the First Intern. Nonlinear Dynamics Conf., NODYCON 2019* Vol. 3 (Eds W Lacarbonara et al.) (Cham: Springer, 2020) p. 131, https://doi.org/10.1007/978-3-030-34724-6_14
11. Mel'nichenko V M, Sladkov A M, Nikulin Yu N *Russ. Chem. Rev.* **51** 421 (1982); *Usp. Khim.* **51** 736 (1982)
12. Dong X et al. *Proc. Natl. Acad. Sci. USA* **119** e2117416119 (2022)
13. Berghoff D et al. *Nat. Commun.* **12** 5719 (2021)
14. Frey Ph, Rachel S *Sci. Adv.* **8** eabm7652 (2022)
15. Kudashkin D V, Nikolaev S V, Yugai K N *Vestn. Omsk. Univ.* **21** (3) 39 (2016)
16. Kutrovskaya S et al. *Nanomaterials* **11** 763 (2021)
17. Compañó R, Molenkamp L, Paul D J (Eds) "Technology Roadmap for Nanoelectronics," Technical Report, 2nd ed. (Brussels: European Commission, 2000) http://dx.doi.org/10.13140/RG.2.2.33846.06727
18. Downer M C et al. *Int. J. Thermophys.* **14** 361 (1993)
19. Onari S, Kontani H *Phys. Rev. Lett.* **128** 066401 (2022); arXiv:2011.01158
20. Pan B et al. *Sci. Adv.* **1** e1500857 (2015)
21. Matyushkin Ya et al. *Appl. Phys. Lett.* **120** 083104 (2022)
22. Wang Q et al. *Nat. Mater.* **15** 159 (2016)
23. Landau L D, Lifshitz E M *Electrodynamics of Continuous Media* (Oxford: Pergamon Press, 1984); Translated from Russian: *Elektrodinamika Sploshnykh Sred* (Moscow: Fizmatlit, 2005)
24. Abrikosov A A *Fundamentals of the Theory of Metals* (Mineola, NY: Dover Publ., 2017); Translated from Russian: *Osnovy Teorii Metallov* (Moscow: Fizmatlit, 2010)
25. Arakelian S M et al. *Vvedenie v Femtonanofotoniku*: *Fundamental'nye Osnovy i Lazernye Metody Upravlyaemogo Poluchenia i Diagnostiki Nanostrukturirovannykh Materialov* (Introduction to Femtonanophotonics: Fundamental Principles and Laser Methods for Controlled Production and Diagnostics of Nanostructured Materials) (Exec. Ed. S M Arakelian) (Moscow: Logos, 2015)
26. Bagayev S N et al. *Bull. Russ. Acad. Sci. Phys.* **84** 1427 (2020); *Izv. Ross. Akad. Nauk Fiz.* **84** 1682 (2020)
27. Khorkov K S, Prokoshev V G, Arakelian S M *J. Adv. Mater. Technol.* **6** (2) 101 (2021)
28. Arakelian S M et al. *Opt. Quantum Electron.* **52** 202 (2020)
29. Khudaiberganov T A et al. *J. Phys. Conf. Ser.* **1164** 012008 (2019)
30. Chestnov I Yu, Khudaiberganov T A, Arakelian S M *J. Phys. Conf. Ser.* **1164** 012005 (2019)
31. Khudaiberganov T A, Chestnov I Yu, Arakelian S M *Appl. Phys. B* **128** 117 (2022)
32. Sobolev M M et al. *Semiconductors* **42** 305 (2008); *Fiz. Tekh. Poluprovodn.* **42** 311 (2008)
33. Antipov A A et al. *Bull. Russ. Acad. Sci. Phys.* **80** 818 (2016); *Izv. Ross. Akad. Nauk Fiz.* **80** 896 (2016)
34. Butko V Yu, DiTusa J F, Adams P W *Phys. Rev. Lett.* **84** 1543 (2000)
35. Skopelitis P et al. *Phys. Rev. Lett.* **120** 107001 (2018)
36. Kutrovskaya S et al. *Nano Lett.* **20** 6502 (2020)
37. Onari S, Kontani H *Phys. Rev. Lett.* **128** 066401 (2022)

38. Orekhov N, Logunov M *Carbon* **192** 179 (2022)
39. Kaiser K et al. *Science* **365** 1299 (2019)
40. Hashimoto T et al. *Sci. Adv.* **6** eabb9052 (2020)
41. Bongiovanni G et al. *Nanoscale Adv.* **3** 5277 (2021)
42. Whittaker A G *Science* **200** 763 (1978)
43. Prokoshev V G et al. *Izv. Ross. Akad. Nauk Fiz.* **61** 1560 (2016)
44. Sladkov A M *Karbin — Tret'ya Allotropnaya Forma Ugleroda* (Carbyne: the Third Allotropic Form of Carbon) (Moscow: Nauka, 2003)
45. Heimann R B, Evsyukov S E, Kavan L (Eds) *Carbyne and Carbynoid Structures* (Dordrecht: Kluwer Acad., 1999)
46. Guseva M B et al., US Patent 6,454,797 B2 (2022); Bloom J et al., US Patent 6,335,350 B1 (2002)
47. Sun Q et al. *J. Am. Chem. Soc.* **138** 1106 (2016)
48. Babaev V G et al. *Poverkhnost Rentgen. Sinkhrotron. Neitron. Issled.* (3) 16 (2004)
49. Rice M J et al. *Phys. Rev. B* **34** 4139 (1986)
50. Misurkin I A, Ovchinnikov A A *Russ. Chem. Rev.* **46** 967 (1977); *Usp. Khim.* **46** 1835 (1977)
51. Khvostov V V et al. *Moscow Univ. Phys. Bull.* **67** (1) 71 (2012); *Vestn. Mosk. Univ. Ser. 3. Fiz. Astron.* (1) 78 (2012)
52. Leider H R, Krikorian H, Young D A *Carbon* **11** 555 (1973)
53. Evseev V N, Kirillin A V, Sheindlin M A *Promyshl. Teplotekh.* **4** (3) 87 (1982)
54. Kirillin A V et al. *High Temp.* **23** 557 (1985); *Teplofiz. Vys. Temp.* **23** 699 (1985)
55. Glukhova O E, Slepchenkov M M, Asanov K R *Semiconductors* **54** 1616 (2020); *Fiz. Tekh. Poluprovod.* **54** 1355 (2020)
56. Hamad A H "Effects of different laser pulse regimes (nanosecond, picosecond and femtosecond) on the ablation of materials for production of nanoparticles in liquid solution," in *High Energy and Short Pulse Lasers* (Ed. R Viskup) (London: IntechOpen, 2016) https://doi.org/10.5772/63892
57. Shugaev M V et al. *MRS Bull.* **41** 960 (2016)
58. Ionin A A, Kudryashov S I, Samokhin A A *Phys. Usp.* **60** 149 (2017); *Usp. Fiz. Nauk* **187** 159 (2017)
59. Georgakilas V et al. *Chem. Rev.* **115** 4744 (2015)
60. Melezhyk A V, Tkachev A G *Nanosyst. Phys. Chem. Math.* **5** 294 (2014)
61. Liu P et al. *Nano Lett.* **8** 2570 (2008)
62. Mortazavi S Z , Parvin P , Reyhani A *Laser Phys. Lett.* **9** 547 (2012)
63. Pilipetskii N F, Rustamov A R *JETP Lett.* **2** 55 (1965); *Pis'ma Zh. Eksp. Teor. Fiz.* **2** 88 (1965)
64. Cataldo F *Carbon* **42** 129 (2004)
65. Kresin V Z, Ovchinnikov Yu N *Phys. Usp.* **51** 427 (2008); *Usp. Fiz. Nauk* **178** 449 (2008)
66. Kresin V V, Ovchinnikov Yu N *Phys. Rev. B* **73** 115412 (2006)
67. Bianco A et al. *Carbon* **132** 785 (2018)
68. Tasis D et al. *Chem. Rev.* **106** 1105 (2006)
69. Rao C N R et al. *Angew. Chem. Int. Ed.* **48** 7752 (2009)
70. Kogan E *Graphene* **2** (2) 74 (2013)
71. Liu M et al. *ACS Nano* **7** 10075 (2013)
72. Casari C S et al. *Nanoscale* **8** 4414 (2016)
73. Kibis O V, Parfitt D G W, Portnoi M E *Phys. Rev. B* **71** 035411 (2005)
74. Kavan L et al. *Carbon* **33** 1321 (1995)
75. Kneipp K et al. *Phys. Rev. Lett.* **84** 3470 (2000)
76. Xiao J, Li J, Yang G *Small* **13** 1603495 (2017)
77. Reber C et al. *J. Phys. Chem.* **95** 2127 (1991)
78. Landau L D, Lifshitz E M *Statistical Physics* Vol. 1 (Oxford: Pergamon Press, 1980); Translated from Russian: *Statisticheskaya Fizika* Pt. 1 (Moscow: Fizmatlit, 2002)
79. Zhao X et al. *Phys. Rev. Lett.* **90** 187401 (2003)
80. Chalifoux W A, Tykwinski R R *Nat. Chem.* **2** 967 (2010)
81. Ma C R, Xiao J, Yang G W *J. Mater. Chem. C* **4** 4692 (2016)
82. Kutrovskaya S V et al. *Sci. Rep.* **10** 9709 (2020)
83. Shaver J, Kono J *Laser Photon. Rev.* **1** 260 (2007)
84. Artyukhov V I, Liu M, Yakobson B I *Nano Lett.* **14** 4224 (2014)
85. Khoo K H et al. *Nano Lett.* **8** 2900 (2008)
86. Zanolli Z, Onida G, Charlier J-C *ACS Nano* **4** 5174 (2010)
87. Zeng M G et al. *Appl. Phys. Lett.* **96** 042104 (2010)
88. Akdim B, Pachter R *ACS Nano* **5** 1769 (2011)
89. Belankov A B, Stolbov V Yu *Sibirsk. Zh. Industr. Matem.* **8** (12) 12 (2005)
90. Bukharov D N, Kucherik A O, Arakelyan S M *J. Phys. Conf. Ser.* **1331** 012017 (2019) https://doi.org/10.1088/1742-6596/1331/1/012017
91. Bukharov D N et al. *J. Phys. Conf. Ser.* **1331** 012008 (2019) https://doi.org/10.1088/1742-6596/1331/1/012008
92. Arakelian S M et al., in *New Trends in Nonlinear Dynamics. Proc. of the First Intern. Nonlinear Dynamics Conf., NODYCON 2019* Vol. 3 (Eds W Lacarbonara et al.) (Cham: Springer, 2020) p. 121, https://doi.org/10.1007/978-3-030-34724-6_13
93. Richardella A et al. *Science* **327** 665 (2010)
94. Gantmakher V F *Electrons and Disorder in Solids* (Oxford: Oxford Univ. Press, 2005); Translated from Russian: *Elektrony v Neuporyadochennykh Sredakh* (Moscow: Fizmatlit, 2013)
95. Ignatov A N *Nanoelektronika. Sostoyanie i Perspektivy Razvitiya* (Nanoelectronics. Status and Development Prospects) (Moscow: Flinta, 2012)
96. Dragunov V P, Neizvestnyi I G, Gridchin V A *Osnovy Nanoelektroniki* (Fundamentals of Nanoelectronics) (Moscow: Logos, 2011)
97. Prazdnikov Yu E et al. *Moscow Univ. Phys. Bull.* **59** (5) 26 (2004); *Vestn. Mosk. Univ. Ser. 3 Fiz. Astron.* (5) 37 (2004)
98. Prazdnikov Yu E et al. *J. Russ. Laser Res.* **26** 245 (2005)
99. Prazdnikov Yu *J. Mod. Phys.* **2** 845 (2011)
100. Ivanenko I P, Krasnoshchekov S V, Pavlikov A V *Semiconductors* **52** 907 (2018); *Fiz. Tekh. Poluprovodn.* **52** 768 (2018)
101. Bukharov D N, Kucherik A O, Arakelian S M *J. Adv. Mater. Technol.* **8** (3) 227 (2023)
102. Huang E W et al. *Science* **358** 1161 (2017)
103. Ferini G, Baratta G A, Palumbo M E *Astron. Astrophys.* **414** 757 (2004)
104. Lozovik Yu E, Popov A M *Phys. Usp.* **40** 717 (1997); *Usp. Fiz. Nauk* **167** 751 (1997)
105. Samyshkin V et al. *Opt. Quantum Electron.* **51** 394 (2019)
106. Yao K-X, Zhang Z, Chin C *Nature* **602** 68 (2022)
107. Briggeman M et al. *Science* **367** 769 (2020)
108. Faoro L, Feigel'man M V, Ioffe L *Ann. Physics* **409** 167916 (2019)
109. Punnoose A, Finkel'stein A M *Science* **310** 289 (2005)
110. Yugai K N *Vestn. Omsk. Univ.* (2) 104 (2013)
111. Wu H et al. *Nature* **604** 653 (2022)
112. Sedov E et al. *Sci. Rep.* **10** 8131 (2020)
113. Sedov E, Arakelian S, Kavokin A *Sci. Rep.* **11** 22382 (2021)
114. Chestnov I Y, Arakelian S M, Kavokin A V *New J. Phys.* **23** 023024 (2021)
115. Feynman R P, Hibbs A R, Styer D F *Quantum Mechanics and Path Integrals* Emended ed. (Mineola, NY: Dover Publ., 2010)
116. Frydman A *Physica C* **391** 382 (2003)
117. Kavokin A et al. *Superlattices Microstruct.* **111** 335 (2017)
118. Sadakov A V, Sobolevskii O A, Pudalov V M *Phys. Usp.* **65** 1313 (2022); *Usp. Fiz. Nauk* **192** 1409 (2022)
119. Marik S et al. *Phys. Rev. Mater.* **3** 060602 (2019)
120. Kang M et al. *Nat. Phys.* **18** 301 (2022)
121. Meng Y et al. *Nat. Commun.* **14** 2431 (2023)
122. Grigoriev I S, Meilikhov E Z (Eds) *Handbook of Physical Quantities* (Boca Raton, FL: CRC Press, 1997); Translated from Russian: *Fizicheskie Velichiny*: *Spravochnik* (Moscow: Energoatomizdat, 1991)
123. Kucherik A et al. *Opt. Spectrosc.* **121** 263 (2016); *Opt. Spektrosk.* **121** 285 (2016)
124. Smirnov B M *Phys. Usp.* **29** 481 (1986); *Usp. Fiz. Nauk* **149** 177 (1986)
125. Aleksandrov D V, Galenko P K *Phys. Usp.* **57** 771 (2014); *Usp. Fiz. Nauk* **184** 833 (2014)
126. Wang E et al. *Nat. Commun.* **14** 7233 (2023)
127. Veselov D A et al. *J. Luminescence* **263** 120164 (2023)